

DIPLOMA THESIS

DEVELOPMENT OF AN MRI-COMPATIBLE ECG
SYSTEM

CSABA HAJDU

SUPERVISORS

Dr Dávid Légrády
BME

Béla Mihalik
Mediso



Budapest University of Technology and Economics
Faculty of Natural Sciences
Institute of Nuclear Techniques
May 2012

COLOPHON

This thesis project was executed within the framework of the Medical Physics specialization of the Physics MSc course at the Institute of Nuclear Techniques, Faculty of Natural Sciences, Budapest University of Technology and Economics.

This document was typeset using the typographical look-and-feel `classicthesis` developed by André Miede. The style was inspired by Robert Bringhurst's seminal book on typography "*The Elements of Typographic Style*". `classicthesis` is available for both \LaTeX and \LyX :

<http://code.google.com/p/classicthesis/>

ÖNÁLLÓSÁGI NYILATKOZAT (DECLARATION OF INDEPENDENT WORK)

Kijelentem, hogy jelen szakdolgozat saját munkám eredménye, azt önállóan, nem megengedett segédeszköz igénybevétele nélkül készítettem el. A szakdolgozatban csak a megadott forrásokat használtam fel. Minden olyan részt, amelyet szó szerint, vagy azonos értelemben, de átfogalmazva más forrásból vettem, egyértelműen, a forrás megadásával jelöltem.

Budapest, 2012. május

Hajdu Csaba

ABSTRACT

Cardiac gating is an important technique used in many different modalities of medical imaging to eliminate artifacts resulting from the motion of the heart. It is often implemented with the use of an electrocardiograph (ECG).

This thesis project was executed at Mediso Medical Imaging Systems. The main objective was the development of an ECG system aimed at cardiac gating, to be used in the pre-clinical (small animal) and clinical (human) imaging devices of the company.

The ECG system is based on a microcontroller and an ECG-specific analog frontend. Prototype hardware was created using development kits and the appropriate firmware was developed. Since the tests carried out with the prototype system confirmed the suitability of the concept, the final hardware was designed. The process is explained in detail.

Cardiac gating also finds use in Magnetic Resonance Imaging (MRI), but this causes challenges in ECG acquisition. Measurements were carried out to assess the usability of the prototype system in MRI. These results are also reported.

KIVONAT

A szívkapuzás fontos technika, amelyet számos különböző orvosi képalkotó modalitás esetében használnak a szív mozgásából eredő műtermékek kiküszöbölésére. A szívkapuzást gyakran elektrokardiográf (EKG) használatával valósítják meg.

Ez a diplomamunka a Mediso Orvosi Berendezés Fejlesztő és Szerviz Kft.-nél készült. A fő célja egy szívkapuzásra szolgáló rendszer kifejlesztése volt, a vállalat preklinikai (kisállat) és klinikai (humán) képalkotó készülékeivel való használatra.

Az EKG rendszer egy mikrokontrolleren és egy EKG-specifikus analóg frontend áramkörön alapul. Fejlesztőkészletek felhasználásával prototípus hardvert alkottam, és kifejlesztettem az azon futó szoftvert. A prototípus rendszerrel lefolytatott tesztek alátámasztották, hogy az elképzelés megfelel a célnak, így megterveztük a végleges hardvert. Ezt a folyamatot a dolgozat részletesen leírja.

Szívkapuzást mágneses rezonancia képalkotó berendezésben (MRI-ben) is alkalmaznak, de ebben az esetben kihívást jelent az EKG mérése. A prototípus rendszer MRI-ben való használhatóságának vizsgálatára méréseket hajtottam végre, amelyek leírása szintén szerepel a dolgozatban.

ACKNOWLEDGMENTS

I would like to express my gratitude to all those people who have contributed to the completion of this project with their assistance and encouragement.

I am extremely grateful to my supervisors, Dr Dávid Légrády and Béla Mihalik for their invaluable support from the first steps of the project to the very end.

Many thanks to Miklós Czeller for his assistance in writing this thesis and to Attila Lantos for some truly great ideas that helped me out of tight spots. It is a pleasure to have had a chance to cooperate with Sándor Török in the design of the hardware. I really appreciate the help of Magor Babos, Sándor Hóbor, Péter Koncz, Domokos Máthé and Zoltán Nyitrai in the organization and execution of small animal ECG measurements.

I am grateful to all the colleagues in my office for an inspiring working environment. I am also very thankful to everyone else at Mediso who lended a hand during my work. Special thanks to the management of the company for letting me tackle this demanding project.

Last but not least, this work can only be dedicated to my family for the love, support and inspiration they've given me all the way through.

CONTENTS

1	INTRODUCTION	1
1.1	Electrocardiography (ECG)	1
1.1.1	Physiological background	1
1.1.2	Recording an ECG	2
1.2	Cardiac gating	3
1.3	ECG in MRI	4
2	SPECIFICATIONS	5
2.1	Specifications of the ECG system	6
3	PROTOTYPING	8
3.1	Choice of architecture	8
3.1.1	The ADS1298R IC	9
3.2	The ECG prototype	9
3.2.1	The ADS1258 MDK	9
3.2.2	The ADS1298R ECG FE-PDK	10
3.2.3	The ECG prototype system	11
3.3	Firmware development	12
3.3.1	The firmware of the ADS1258 MDK	12
3.3.2	The firmware of the ECG prototype system	14
4	HARDWARE DESIGN	20
4.1	Choice of microprocessor	20
4.2	Hardware design considerations	21
4.2.1	Patient protection	22
4.2.2	Power supplies	22
4.2.3	ECG hardware	24
4.2.4	Small animal respiratory measurement	25
4.2.5	Microcontroller unit	26
4.2.6	Communication interfaces	26
4.3	The hardware	27
5	MEASUREMENTS	28
5.1	ECG signal acquisition	28
5.1.1	ECG simulator	28
5.1.2	Human ECG	30
5.1.3	Small animal ECG	30
5.2	Performance in MRI	33
5.2.1	Initial measurements	34
5.2.2	Small animal measurements	34
5.2.3	Discussion	37
6	SUMMARY	39
6.1	Accomplishments	39
6.2	Possibilities of improvement	39
A	APPENDIX	40

LIST OF FIGURES

Figure 1.1	Schematic representation of normal ECG.	2
Figure 2.1	Block diagram of the ECG system.	5
Figure 3.1	Block diagram of the ADS1298R.	9
Figure 3.2	Photo of the ADS1298R ECG FE-PDK.	10
Figure 3.3	Photo of the ECG prototype system.	11
Figure 3.4	IIR filter frequency response of the ADS1258 MDK.	13
Figure 3.5	FIR filter frequency response of the ADS1258 MDK.	13
Figure 3.6	Flowchart of the ECG prototype system firmware.	15
Figure 3.7	Screenshot of the PC application for ECG display.	16
Figure 3.8	Frequency response of the DC removal filter.	17
Figure 3.9	Response of the human band-pass filter.	18
Figure 3.10	Response of the animal band-pass filter.	18
Figure 3.11	Impulse response of the human band-pass filter.	18
Figure 3.12	Frequency response of the notch filter.	19
Figure 4.1	The architecture of the Concerto MCU family.	21
Figure 4.2	Frequency response of the antialiasing filter.	25
Figure 4.3	Rendered visualization of the ECG board.	27
Figure 5.1	ECG simulator output.	29
Figure 5.2	ECG simulator output, corrupted by 50Hz noise.	29
Figure 5.3	Human ECG recording.	30
Figure 5.4	Human stress ECG recording.	31
Figure 5.5	The anesthetized rat fitted with ECG electrodes.	32
Figure 5.6	Rat ECG recording.	32
Figure 5.7	Hamster ECG recording.	33
Figure 5.8	Background spectrum measured inside the MRI.	35
Figure 5.9	Spectrum of a hamster ECG within MRI.	36
Figure 5.10	Spectrum of a hamster ECG within MRI, zoomed.	36
Figure 5.11	Spectrum of a hamster ECG during MRI sequence.	37

LIST OF TABLES

Table 2.1	Design parameters of the ECG system.	7
-----------	--	---

LISTINGS

Listing A.1	Configuration of the ADS1298R.	40
-------------	--	----

ACRONYMS

AD	Analog-to-Digital
ADC	Analog-to-Digital Converter
AFE	Analog Frontend
CT	Computed Tomography
CAN	Controller Area Network
CMRR	Common-Mode Rejection Ratio
DSP	Digital Signal Processor
ECG	electrocardiograph
EVM	Evaluation Module
FIR	Finite Impulse Response
GPIO	General Purpose Input/Output
IC	Integrated Circuit
IIR	Infinite Impulse Response
LCD	Liquid Crystal Display
MCU	Microcontroller Unit
MDK	Medical Development Kit
MRI	Magnetic Resonance Imaging
PDK	Performance Demonstration Kit
PET	Positron Emission Tomography
PGA	Programmable Gain Amplifier
PSRR	Power Supply Rejection Ratio

RLD	Right Leg Drive
SAR	Successive Approximation Register
SPI	Serial Peripheral Interface
TI	Texas Instruments
UART	Universal Asynchronous Receiver/Transmitter
USB	Universal Serial Bus
WCT	Wilson Central Terminal

INTRODUCTION

This thesis describes the development of an electrocardiograph (ECG) system designed for cardiac gating. This chapter is aimed at highlighting the significance of cardiac gating in pre-clinical (animal) and clinical (human) medical imaging.

Section 1.1 discusses electrocardiography based on [1]. Assuming a basic knowledge of the anatomy of the heart, the physiological background of human ECG is explored, without delving into the clinical significance of ECG traces. Next, the practical aspects of ECG recording relevant to this project are reviewed.

Section 1.2 gives an overview of cardiac gating, and Section 1.3 deals with the challenges of ECG measurement in Magnetic Resonance Imaging (MRI) machines.

1.1 ELECTROCARDIOGRAPHY (ECG)

1.1.1 *Physiological background*

As the heart undergoes depolarization and repolarization during the cardiac cycle, the electrical currents that are generated spread not only within the heart, but also throughout the body. This electrical activity generated by the heart can be measured by an array of electrodes placed on the body surface. The recorded tracing is called an electrocardiogram (ECG, or EKG). Figure 1.1 shows the schematic representation of a "typical" human ECG tracing. The different waves that comprise the ECG represent the sequence of depolarization and repolarization of the atria and ventricles.

The P wave represents the wave of depolarization that spreads from the sinoatrial (SA) node throughout the atria, and is usually 80-100 ms in duration. The brief isoelectric period after the P wave represents the time in which the impulse is traveling within the atrioventricular (AV) node and the bundle of His.

The period of time from the onset of the P wave to the beginning of the QRS complex is termed the P-R interval, which normally ranges from 0.12 to 0.20 seconds in duration. This interval represents the time between the onset of atrial depolarization and the onset of ventricular depolarization.

The QRS complex represents ventricular depolarization. Heart rate can be calculated by determining the time interval between QRS complexes. The duration of the QRS complex is normally 0.06 to 0.1 sec-

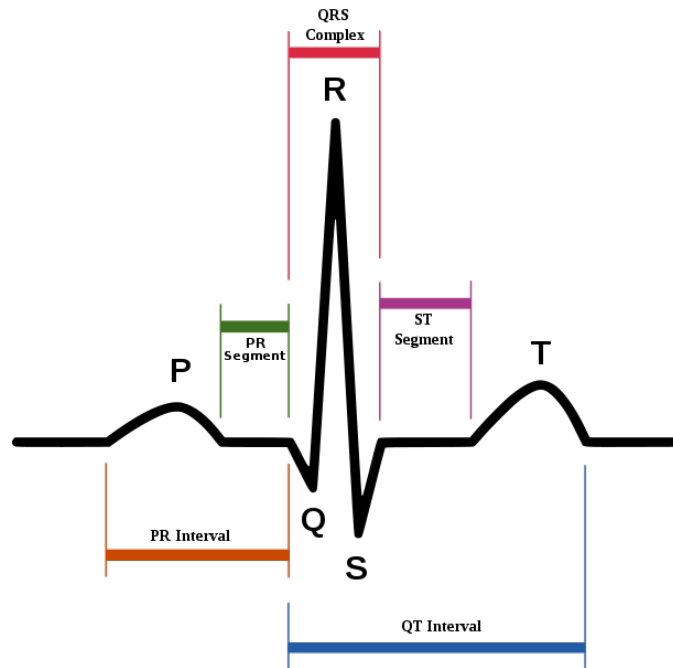


Figure 1.1: Schematic representation of normal ECG. Courtesy of Wikipedia.

onds. This relatively short duration indicates that ventricular depolarization normally occurs very rapidly.

The isoelectric period (ST segment) following the QRS is the time at which the entire ventricle is depolarized.

The T wave represents ventricular repolarization and is longer in duration than depolarization, since conduction of the repolarization wave is slower than the wave of depolarization.

The Q-T interval represents the time for both ventricular depolarization and repolarization to occur. This interval can range from 0.2 to 0.4 seconds depending upon heart rate.

There is no distinctly visible wave representing atrial repolarization in the ECG because it occurs during ventricular depolarization. Because the wave of atrial repolarization is relatively small in amplitude, it is masked by the much larger ventricular-generated QRS complex.

1.1.2 Recording an ECG

By convention, in a 5-electrode ECG configuration, electrodes are positioned on each arm and leg, and one electrode is placed on the chest. The limb electrodes are referred to as Left Arm (LA), Right Arm (RA), Left Leg (LL) and Right Leg (RL), while the chest electrode is referred to as V_1 . LA, RA, LL and V_1 are used as input electrodes in monitoring the electrical activity of the heart, whereas RL is electrically driven by the Right Leg Drive (RLD) circuitry to reduce the common-mode

voltage on the other electrodes. In general, the RL signal is obtained as the average of the other limb electrodes.

The conventional **ECG leads** are formed from the *electrode* signals. The **ECG leads** are subdivided into the following categories:

- Standard limb leads: I, II, III
- Augmented limb leads: aVL, aVR, aVF
- Chest lead: V₁

The leads are formed according to the following rules:

$$\begin{aligned}
 I &= LA - RA \\
 II &= LL - RA \\
 III &= LL - LA \\
 aVL &= LA - \frac{1}{2} \cdot (RA + LL) \\
 aVR &= RA - \frac{1}{2} \cdot (LA + LL) \\
 aVF &= LL - \frac{1}{2} \cdot (LA + RA) \\
 V_1 &= V_1 - \frac{1}{3} \cdot (LA + RA + LL)
 \end{aligned}$$

The standard limb leads are *bipolar* because the lead voltage is measured between two electrodes, while the other leads are *unipolar* because they are measured with respect to the Wilson Central Terminal (**WCT**) voltage, which is defined as $V_W = \frac{1}{3} \cdot (LA + RA + LL)$.

In practice, **ECG** signal acquisition may be implemented with differential amplifiers. In this case, the standard limb leads may be obtained directly by connecting the appropriate electrodes to the inputs of the differential amplifiers. The chest lead may be obtained by generating the **WCT** voltage and measuring the chest electrode with respect to it. The augmented limb leads may be calculated digitally from the other leads.

In the case of small animal measurements, three electrodes are generally used. The electrode configuration may be LA, RA and LL, or alternatively, LA, RA and RL to provide feedback for common-mode signal reduction.

1.2 CARDIAC GATING

Cardiac gating is a technique used to reduce artifacts due to heart motion in medical imaging.

The heart is in motion during the cardiac cycle. It completes the contraction required for its pump function during the systolic phase,

then relaxes in the diastolic phase. Regardless of the imaging modality in use, it is desirable to create images of the heart while it is stationary in order to minimize motion artifacts. The diastolic periods of lesser cardiac motion are ideal candidates for artifact-free imaging, however, the temporal resolution of current imaging techniques is not sufficient for the creation of images in a single stationary period. This problem can be addressed with the use of ECG-synchronized techniques to record and combine data from multiple stationary periods for motion-free imaging.

The occurrence of the QRS complex in the ECG corresponds to the period of greatest heart motion. Therefore, by recording QRS triggers along with the image data, data from the periods of lesser motion can subsequently be extracted for the reconstruction of motion-free images (retrospective ECG gating). Moreover, the occurrence of QRS complexes can be predicted on the fly from the previous ECG data, which can be used in Computed Tomography (CT) imaging for reducing the output power of the X-ray tube during systole in order to reduce patient dose (prospective ECG triggering) [2].

Cardiac gating has been proven to be efficient in cardiac CT and coronary angiography [2], cardiac Positron Emission Tomography (PET) [3] and even in MRI diffusion tensor imaging of the brain [4].

1.3 ECG IN MRI

As discussed above, ECG acquisition in MRI is clinically relevant. However, it is a challenging task.

In addition to the inherent distortion of the ECG waveform in MRI systems operating at high field strengths, the static, gradient and RF electromagnetic fields of the MRI system can cause additional artifacts in the ECG signal [5]. Moreover, the ECG electrode leads may act as antennas, guiding radio-frequency interference into the MRI bore, thereby generating imaging artifacts or even causing image acquisition to fail.

An existing MRI-compatible ECG system for human applications employs long MRI-compatible cables and filtering in order to leave the electronics outside of the MRI chamber [6], but solutions allowing the monitor to be placed near the patient are also available [7, 8].

Solutions also exist for small animal applications [9, 10]. The documentation available on-line reveals very limited detail about these systems, in particular with respect to the MRI architectures and field strengths they are compatible with. However, both systems appear to rely on MRI-compatible ECG electrodes and lead wires, and the elimination of artifacts in the ECG signal by digital filtering.

SPECIFICATIONS

The thesis project was executed at Mediso Medical Imaging Systems, Hungary. The company's specifications for the ECG system project require the development of a modular ECG system. The main module should implement the acquisition of the ECG signals with QRS complex detection, trigger generation and transmission for cardiac gating in pre-clinical and clinical imaging machines, along with pre-clinical respiratory measurement and triggering. The slave module should implement a temperature control loop for small animal systems, measuring and regulating the temperature of the animal bed. Each device should implement two channels, i.e. it should be able to operate with two patients (animals) simultaneously, with a shared microprocessor (see Figure 2.1). Although the possibility to visualize signal waveforms is required, the project is not aimed at the development of a diagnostic quality ECG system.

The thesis deals with the development of the main module, and only describes details pertaining to the ECG functionality.

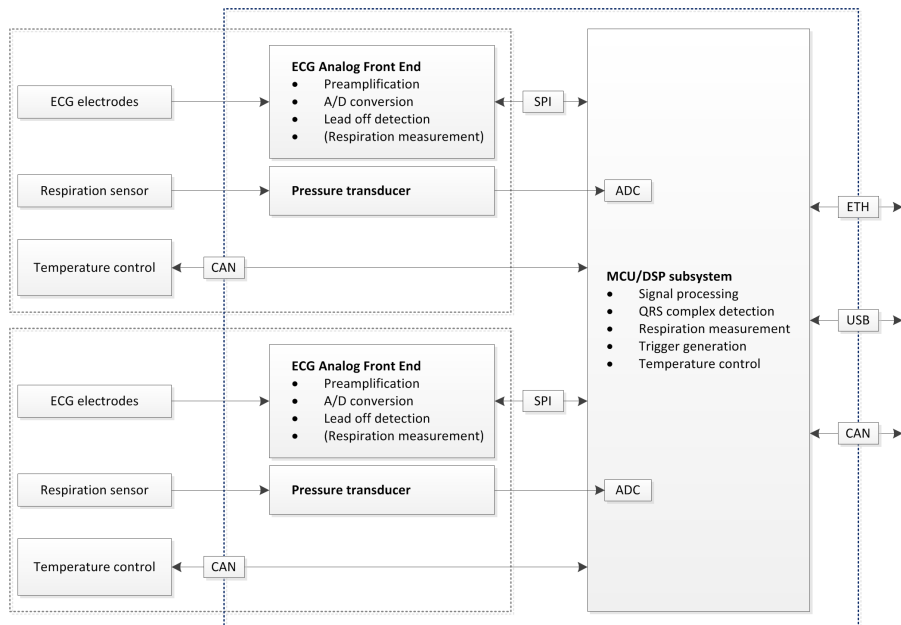


Figure 2.1: Block diagram of the ECG system.

2.1 SPECIFICATIONS OF THE ECG SYSTEM

An excerpt of the original specifications by Mediso follows.

1. Input/output

- Digitization of signals from 4 ECG electrodes in parallel for 7-lead ECG
- RLD bias electrode
- ECG cables with standard connectors should be usable
- Communication interfaces: IEEE 1588 Ethernet, Universal Serial Bus (USB), Controller Area Network (CAN)

2. Electronics, signal processing

- Digitization of human and rat/mouse ECG signals
- Automatic QRS complex detection, trigger generation and transmission
- Configurable ECG preamplifier gain
- Power line interference filter
- Switchable high- and low-pass filters
- Automatic detection and reporting of ECG electrode faults
- Protection against overvoltages from defibrillators

3. Safety

- Patient isolation: at least 4 kV from communication interfaces and power network
- Defibrillator protection: at least 5 kV at inputs
- Compliance with the IEC 60601-2-25 standard for medical electrical equipment

4. Design parameters (see Table 2.1)

Table 2.1: Design parameters of the ECG system.

	Min	Typ	Max
Supply voltage (DC)	9 V	24 V	36 V
Number of ECG electrodes		4 + 1	
Analog preamplification	1x	6x	12x
AD converter resolution	12 bits		
Input bandwidth	0.05 Hz		250 Hz
Low pass filter frequency (human)		35 Hz	
Low pass filter frequency (animal)		75 Hz	
High pass filter frequency		0.05 Hz	
Power line filter notch frequency		50 Hz / 60 Hz	
Input sensitivity	10 μ V		
CMRR	100 dB		
Input voltage range		\pm 300 mV	
Input impedance		20 M Ω	
Input-referred noise			15 μ V
Heart rate (human)			400 bpm
Heart rate (animal)			800 bpm
Trigger latency			100 ms
Trigger jitter			10 ms

PROTOTYPING

3.1 CHOICE OF ARCHITECTURE

Many digital ECG designs are based on discrete electronic components. Depending on the level of complexity used, the entire analog signal processing stage is implemented using numerous separate Integrated Circuits (ICs) up to the point of Analog-to-Digital (AD) conversion. Publicly available examples include simple, 2-electrode ECG monitor circuit designs by Analog Devices [11] and by Texas Instruments (TI) [12], and the ADS1258 Medical Development Kit (MDK) by TI [13].

However, at present several Analog Frontend (AFE) ICs are available that implement a significant portion of the analog functionality required for ECG in one piece of silicon [14]. This might include lead signal preamplification, an RLD DC bias circuit, generation of the WCT voltage used as reference voltage, ECG lead-off detection, respiration measurement over the ECG electrodes and AD conversion.

In order to facilitate hardware development and accelerate the design, I decided to execute the project based on an AFE IC. Two options were commercially available for consideration:

- the ADS119x/129x¹ family by TI,
- the ADAS1000² by Analog Devices.

The features put forward by both candidates are very similar. In contrast to TI's high-end ICs, the ADAS1000 only has 5 input channels, but this would be sufficient to implement the 4+1 electrode ECG required by the specifications (see Chapter 2). However, the ADAS1000 is still in the pre-release phase at the time of writing this document, therefore TI's offer was the reasonable choice.

The TI ADS129x family offers better performance than the ADS119x, notably in terms of resolution, noise and Common-Mode Rejection Ratio (CMRR). Optionally, it also integrates the possibility to implement respiration measurement over ECG electrodes [15]. Moreover, it is relatively inexpensive, thus it was chosen for development.

The prototyping phase was carried out using an ADS1298R IC, but the final product does not require all the input channels it offers and, depending on the configuration, the respiration capability might also

¹ http://www.ti.com/ww/en/analog/ads1298/index.shtml?DCMP=analog_signalchain_mr&HQS=ads1291-pr

² <http://www.analog.com/en/analog-to-digital-converters/ad-converters/adas1000/products/product.html>

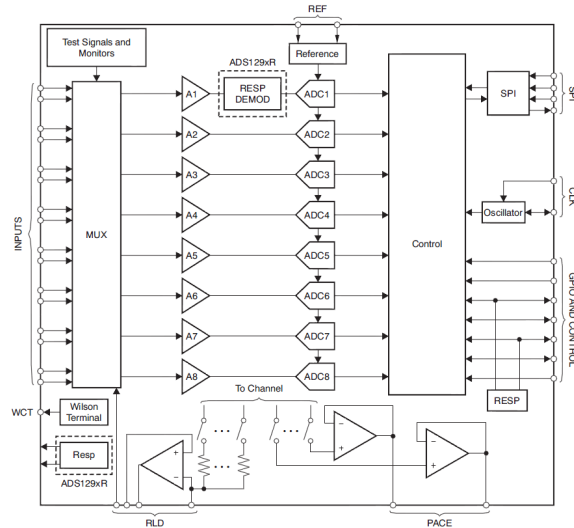


Figure 3.1: Block diagram of the ADS1298R [15].

be unnecessary, so one of the less expensive pin-compatible variants may be used in the end-product.

3.1.1 The ADS1298R IC

The ADS1298R³ is an 8-channel AFE meant for biopotential measurements (see Figure 3.1). It features eight low-noise Programmable Gain Amplifiers (PGAs) and eight high-resolution Analog-to-Digital Converters (ADCs) for fully parallel data acquisition at a wide range of configurable data rates. It offers low power consumption and small input-referred noise alongside a high CMRR. It provides built-in RLD circuitry, lead-off detection and WCT circuitry for ECG. It also integrates support for respiration impedance measurement over ECG electrodes.

The ADS1298R provides a convenient Serial Peripheral Interface (SPI) for configuration and measurement data readout, thus it requires only a limited number of additional digital control signals [15].

3.2 THE ECG PROTOTYPE

3.2.1 The ADS1258 MDK

At the beginning of development, an ECG MDK based on TI's ADS1258⁴ IC was already available at Mediso. This development kit consists of an Evaluation Module (EVM)⁵ by Spectrum Digital based on TI's

³ <http://www.ti.com/product/ads1298r>

⁴ <http://www.ti.com/product/ads1258>

⁵ <http://support.spectrumdigital.com/boards/evm5505/revd/>

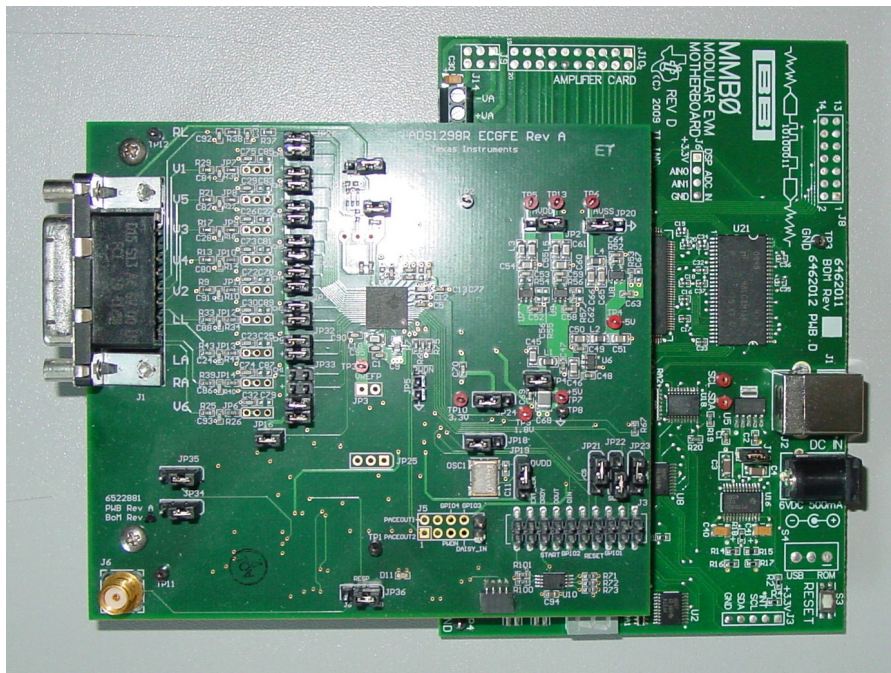


Figure 3.2: Photo of the ADS1298R ECG FE-PDK.

TMS320VC5505⁶ Digital Signal Processor (DSP), and a piggy-back module hosting the ADS1258 and accompanying circuitry. The Performance Demonstration Kit (PDK) also includes the firmware running on the DSP implementing ECG signal acquisition and processing, and a PC application which receives the ECG waveforms over a serial link and plots them.

Since the ADS1258 is merely a 16-channel ADC and all ECG-related functionality is implemented using external components, this IC was not considered for design. However, the TMS320VC5505 EVM has proved to be essential in later development (see Section 3.2.3), and I also reused the PC application supplied with the MDK (see Section 3.3).

3.2.2 The ADS1298R ECG FE-PDK

To start experimenting with the AFE I've chosen, I ordered an ADS1298R PDK. The kit contains the MMB00 Modular EVM motherboard that hosts a TI TMS320VC5509⁷ DSP, and the ADS1298R ECG AFE on a piggy-back board. The assembled system is shown in Figure 3.2.

Once out of the box and wired up to a PC, the demo kit acquired ECG signals perfectly, yet it wasn't usable for further development because of the lack of documentation and development tools for the

⁶ <http://www.ti.com/product/tms320vc5505>

⁷ <http://www.ti.com/product/tms320vc5509>

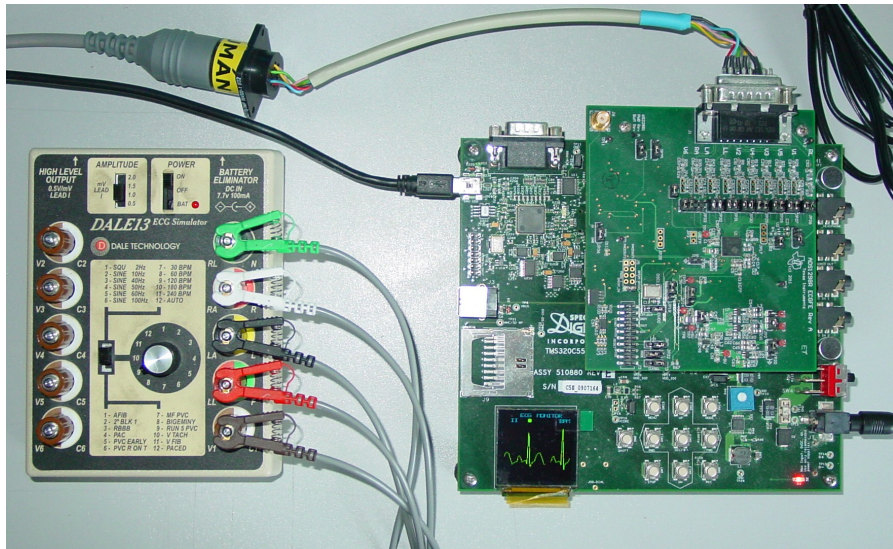


Figure 3.3: Photo of the ECG prototype system connected to an ECG simulator. The acquired ECG waveforms are visible on the LCD display.

MMBo board. According to TI, “The MMBo is not intended to be a full embedded development tool, it is an evaluation platform.”⁸

3.2.3 The ECG prototype system

Fortunately, the two PDKs share the same piggy-back interface, hence mounting the ADS1298R piggy-back module on the TMS320VC5505 EVM is possible. The piggy-back interface provides all the necessary signals for the SPI interface used in the communication with the ADS1298R IC and the digital control signals. Since the EVM offers excellent development and debug support through TI’s Eclipse-based Code Composer Studio suite, it is an ideal platform for a detailed exploration of the features of the ADS1298R AFE. The EVM also features a color AMOLED⁹ Liquid Crystal Display (LCD) and a Universal Asynchronous Receiver/Transmitter (UART) port which were useful for visualizing the ECG waveforms both locally and through data transmitted to a PC (see Section 3.3).

Figure 3.3 shows the ECG prototype system connected to an ECG simulator (see Section 5.1.1). The digitized output of the simulator is displayed on the LCD screen.

⁸ Official comment on http://e2e.ti.com/support/data_converters/precision_data_converters/f/73/t/151713.aspx, retrieved on 09/05/2012.

⁹ Active-matrix organic light-emitting diode.

3.3 FIRMWARE DEVELOPMENT

Since the [ECG](#) prototype system is implemented using the [DSP](#) module of the [ADS1258 MDK](#), several features of its firmware are based on the firmware supplied with the [MDK](#) by [TI](#).

3.3.1 *The firmware of the ADS1258 MDK*

Following are the features of the firmware supplied with the [ADS1258 MDK](#), as listed in [TI](#)'s application note [13]. I also appended brief explanations, mainly focusing on how they relate to the features required in the firmware of the [ECG](#) prototype system (see [Section 3.3.2](#)).

Data acquisition through ADC

The firmware establishes communication with the [ADS1258 IC](#) over the [SPI](#) bus for configuration and data retrieval. The [ADS1298R](#) also has an [SPI](#) interface, however, the protocol is different. In addition to adapting the protocol, I rewrote the entire [SPI](#) implementation in the [ECG](#) prototype system firmware for clarity.

Lead-off detection

[ECG](#) lead-off detection is implemented using external circuitry on the [ADS1258 MDK](#) board. The firmware takes care of the communication with these. Since the [ADS1298R](#) implements lead-off detection internally and the status information can be read out over [SPI](#), this feature is not required in the [ECG](#) prototype system.

DC signal removal

The firmware implements a first-order digital Infinite Impulse Response ([IIR](#)) filter for baseline restoration of the [ECG](#) signal. The frequency response of the filter is shown in [Figure 3.4](#). The filter is implemented in platform-independent C code and I reused it in the prototype firmware almost without modifications.

Multi band-pass filtering

The firmware implements a digital Finite Impulse Response ([FIR](#)) filter. The coefficients of the filter realize a low-pass filter for the elimination of high-frequency noise with a notch for the suppression of power line interference. [Figure 3.5](#) shows the frequency response of the filter with coefficients realizing a notch at 50 Hz.

The [FIR](#) filter is implemented in architecture-specific assembly code. I reused the implementation in the [ECG](#) prototype system firmware with different filter coefficients yielding different filter characteristics.

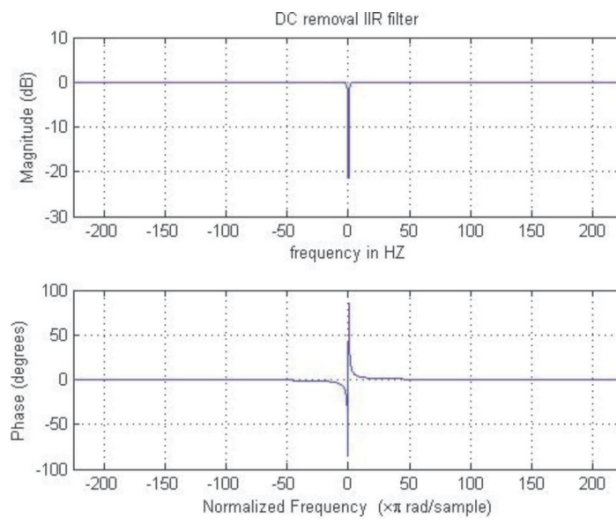


Figure 3.4: Frequency response of the IIR filter of the ADS1258 MDK [13]. The filter suppresses the DC component of the signal for baseline restoration.

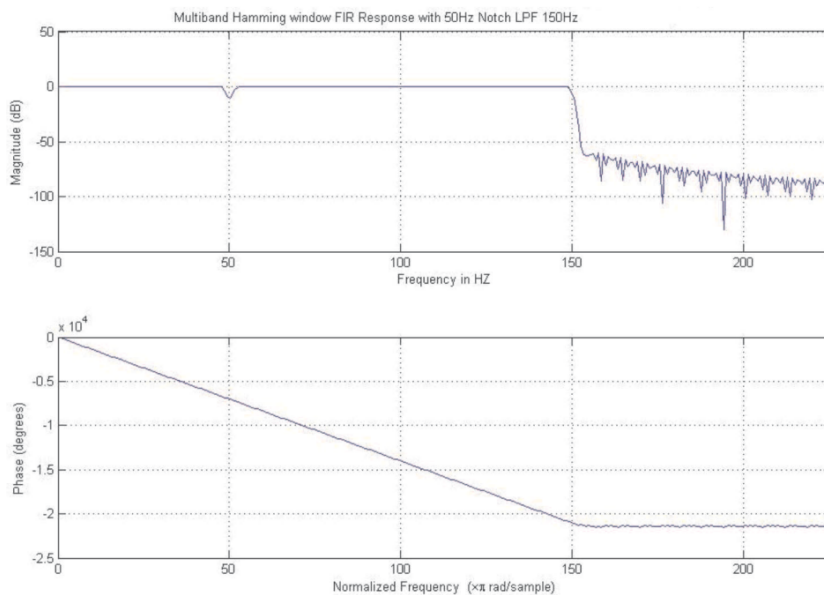


Figure 3.5: Frequency response of the FIR filter of the ADS1258 MDK [13]. The filter has a notch at 50 Hz to suppress power line interference and has a stopband with a very high attenuation above 150 Hz to filter out high frequency noise.

ECG leads formation

The firmware carries out ECG lead formation from the single ended input signals with simple arithmetics according to the rules described in Section 1.1.2. Since the ADS1298R has differential inputs, the arithmetic operations to perform are different.

QRS (heart rate) detection

The firmware implements the detection of the QRS complex (see Section 1.1.1) in the ECG signal for heart rate measurement. QRS detection is a crucial feature required for cardiac gating, but this requires real-time detection with limited latency. However, this algorithm is only aimed at heart rate measurement, it has unacceptably high latency and is unsuitable for the purposes of the ECG system.

Display of ECG data

The acquired ECG waveform is plotted on the AMOLED LCD screen with a possibility to select the ECG lead to plot using the keys of the EVM5505. This feature was useful for demonstration purposes and has been reused in the ECG prototype system with negligible modifications.

UART communication

The acquired ECG data is transmitted over UART to the PC application for display. This feature was also useful for demonstration and has been reused in the ECG prototype system firmware.

3.3.2 The firmware of the ECG prototype system

The main purpose of the ECG system is to issue triggers for gated imaging at the occurrence of QRS complexes with deterministic delay, i.e. limited and unvarying latency, and small jitter (see Chapter 2). The firmware has been designed with this requirement in mind. Most of the project is implemented in platform-independent C code, with the exception of the low-level CPU peripheral drivers and the FIR filter.

The flowchart of the ECG prototype system firmware is shown in Figure 3.6. A detailed description follows.

The main function

The main function performs the initialization of the entire ECG system.

It initializes the peripherals of the DSP: SPI for communication with the ADS1298R, UART for data transfer to the PC, a Successive Approximation Register (SAR) ADC that reads out keypresses for LCD configuration, the LCD for ECG waveform display, and General Purpose

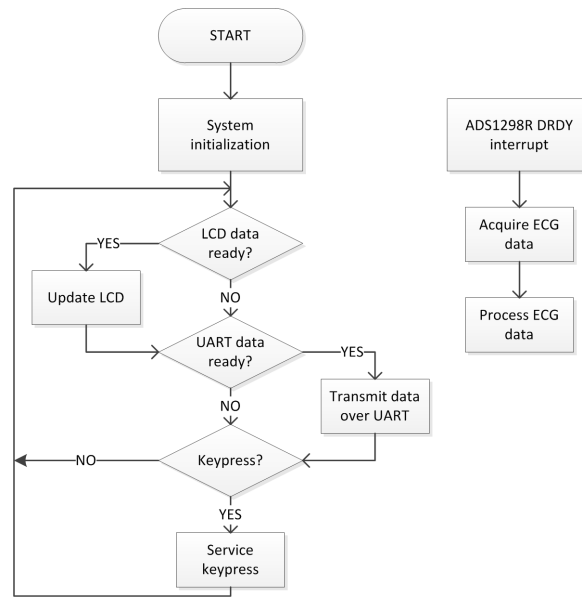


Figure 3.6: Flowchart of the ECG prototype system firmware.

Input/Outputs (GPIOs) for controlling the ADS1298R and debugging features.

It then initializes and configures the ADS1298R AFE. The register settings can be found in Listing A.1 (for detailed explanations, see [15]). The following set of main configuration parameters has proved to be usable in all cases tested so far (see Section 5.1):

- Sample rate set to 1000 SPS by default.
- The gain of all PGAs is set to 6.
- Lead-off detection is enabled for all ECG electrodes.
- The RLD and WCT signals are generated as the average of the LA, RA and LL signals (see Section 1.1.2).

Finally, it enters an infinite loop where, whenever data is available, it plots ECG waveforms to the LCD and transmits ECG data over UART to the PC for display. It also monitors keypresses and updates the LCD display configuration accordingly.

Figure 3.7 shows a screenshot of the PC application. The ECG waveforms and actual measured heart rate of a rat are displayed as acquired by the ECG prototype system. The measurement configuration only included the electrodes necessary for the calculation of Lead I (see Section 5.1.3), thus the waveform displayed for Lead II is calculated and displayed incorrectly and should be considered an arithmetic artifact.

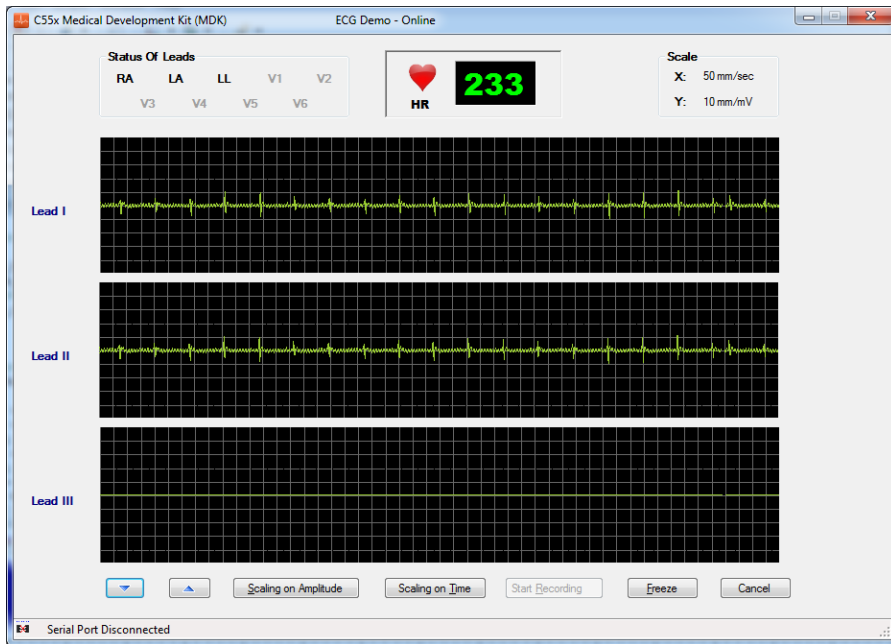


Figure 3.7: Screenshot of the PC application displaying the ECG waveforms and actual measured heart rate of a rat, acquired by the ECG prototype system.

The DRDY interrupt subroutine

The ADS1298R is configured for continuous data acquisition, thus it provides new data at the sampling rate specified in the configuration, signaling its availability through its Data Ready (DRDY) output signal. The prompt response of the ECG system to the availability of new data is ensured by an interrupt mapped to the DRDY signal. Whenever new data is available, the firmware reads it out over the SPI bus, then executes the following steps of processing:

- *Data preprocessing.* Lead-off information is extracted from the status word received from the ADS1298R. The 24-bit output of the ADC is converted to 16-bit resolution by truncation of a configurable number of bits. To allow for a flexible input configuration, the ADC channel values are sorted into an internal buffer according to a changeable map. The input values that contain signal from any disconnected electrode are zeroed out. Based on the lead-off status, one healthy lead is selected for QRS detection.
- *Filtering.*
 - *Baseline restoration.* A first-order IIR filter adapted from the ADS1258 MDK (see Section 3.3.1) is used for suppressing the DC component of the ECG signal. The frequency response of the filter is shown in Figure 3.8.

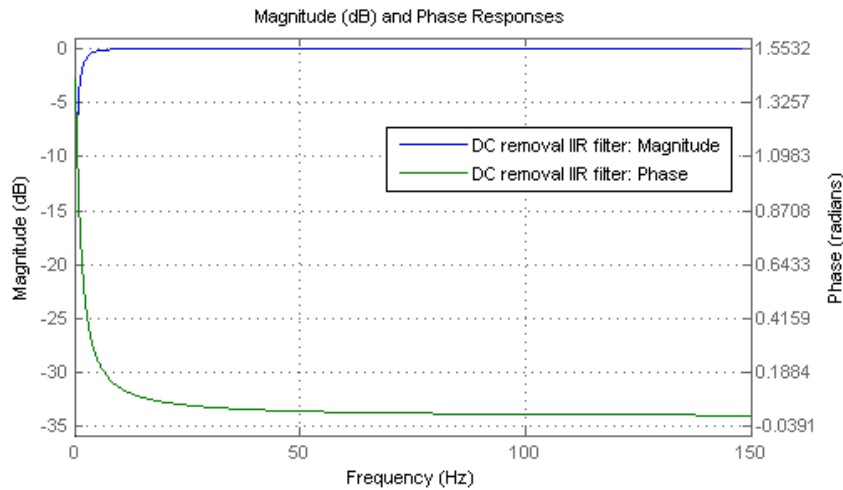


Figure 3.8: Frequency response of the DC removal IIR filter. The filter restores the baseline of the ECG signal.

- *Band-pass filtering.* I reused the FIR filter implementation in the ADS1258 MDK with a set of custom coefficients I designed in Matlab for a 128-tap FIR filter. The lower stopband of the band-pass filter reduces undesirable signal contributions from muscle movement, weakens the P and T waves and softens the QRS complex, but since the project is not aimed at the creation of a diagnostic quality ECG, this is acceptable. The higher stopband is designed to filter out high frequency noise. Figure 3.9 and Figure 3.10 show the frequency response of the filters used in human and small animal applications, respectively (see Chapter 2). Both filters have linear phase in the passband, which is a desirable characteristic since it implies equal delay at all frequencies. FIR filters have a characteristic delay which is determined by the location of the peak of the filter impulse response. Since both filters have this peak at half the number of taps, 64 samples (see Figure 3.11), the delay introduced is 64 ms at 1000 SPS.

Due to the integer arithmetics used in the FIR filter implementation, the filter coefficients were converted from double-precision floating point to integers. As a result, preserving the relatively flat response in the passband, the filters have significant amplification. However, with sufficient care taken to avoid arithmetic overflows, this was very easily compensated.

- *Notch filtering.* Since the stopband of the band-pass filter for preclinical applications lies above the frequency of power line interference, in these applications, a separate filter is required for the suppression of these undesirable contribu-

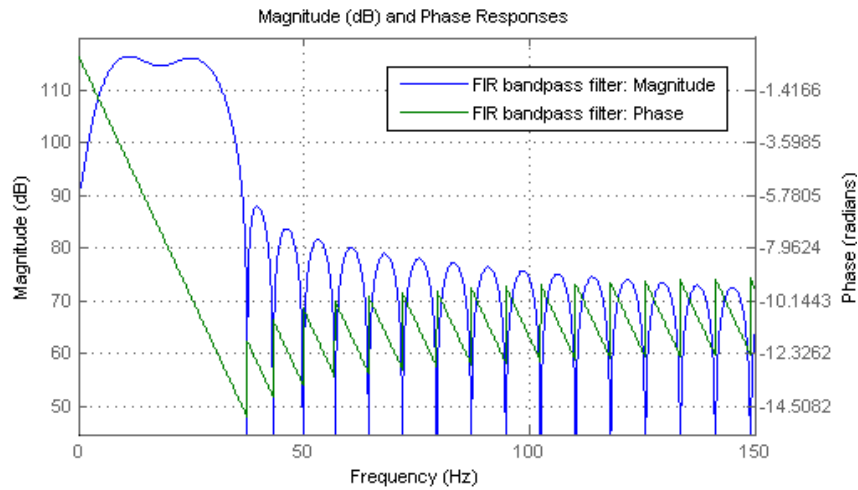


Figure 3.9: Frequency response of the human band-pass FIR filter. Smaller heart rates allow for a lower cutoff frequency.

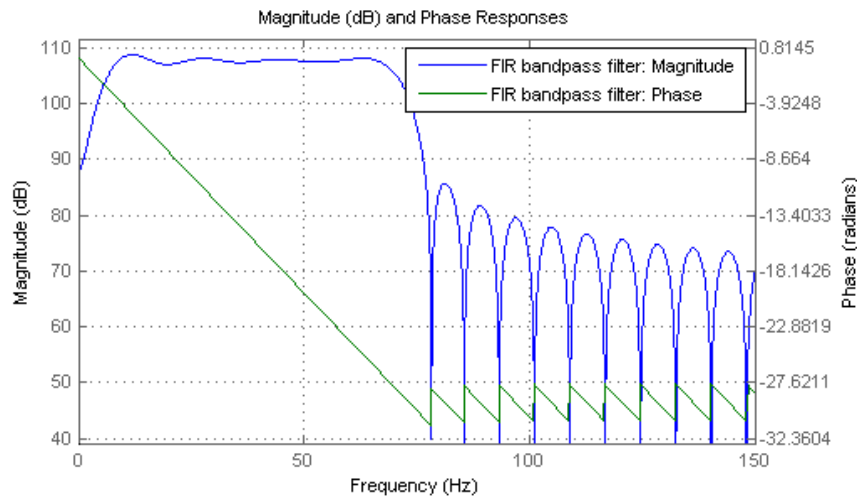


Figure 3.10: Frequency response of the small animal band-pass FIR filter. Higher heart rates require a wider passband.

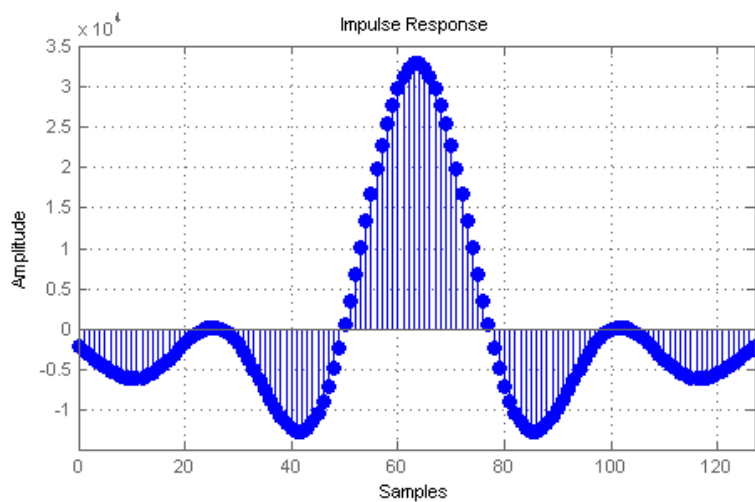


Figure 3.11: Impulse response of the human band-pass FIR filter.

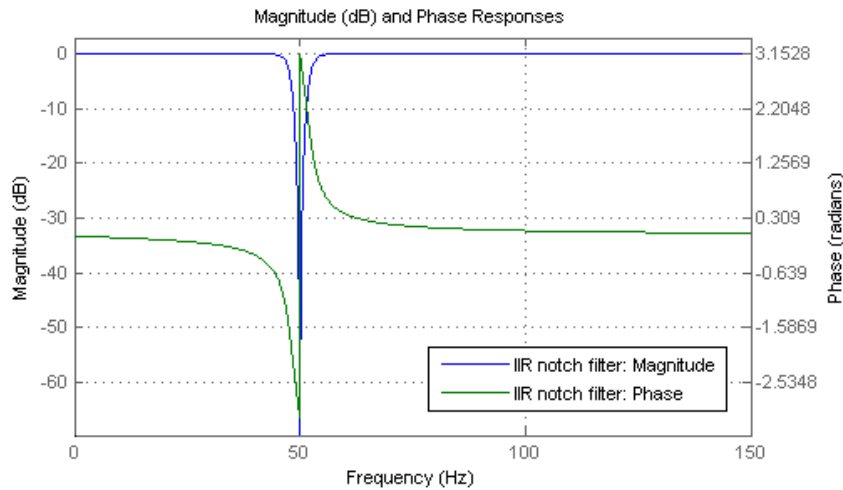


Figure 3.12: Frequency response of the IIR notch filter for power line interference suppression. Notch frequency is 50 Hz. The filter has a relatively blunt notch to reduce transients.

tions. For this purpose, I designed an IIR filter in Matlab. Based on the coefficients obtained, I implemented this filter as a cascade of two second-order IIR stages in platform-independent C code. Figure 3.12 depicts the frequency response of the filter with a 50 Hz notch.

- *QRS detection.* As discussed in Section 3.3.1, the QRS detection algorithm implemented in the ADS1258 MDK is unsuitable for the purposes of the ECG system. Therefore, I implemented a detection algorithm based on the Pan-Tompkins algorithm [16]. The algorithm relies on the previously filtered signal. As mentioned above, the band-pass filter distorts the P and T waves in the ECG signal. It also softens the peak of the QRS complex, however, by subsequent application of a five-point digital derivative filter and squaring its output, the output has proved to be an excellent metric for QRS detection in all cases tested (see Section 5.1). Pan and Tompkins applied a moving window average filter to this signal, which yields a series of pulses and allows for QRS detection through rising edge detection. I simply perform threshold crossing detection on the squared derivative with an adaptive threshold established based on the last five detection amplitudes. Each detection inhibits further detections for a configurable amount of time, thereby avoiding multiple detections of the same QRS complex.
- *UART and LCD flag generation.* Not all samples are sent to the UART and LCD. The ratio of decimation is configurable and the corresponding data ready flags, processed by the main loop, are generated accordingly.

HARDWARE DESIGN

I carried out the hardware design in cooperation with my colleague Sándor Török. Many design choices originate from his professional experience.

4.1 CHOICE OF MICROPROCESSOR

The specification of the project requires the implementation of a variety of communication interfaces (see [Chapter 2](#)). Among those specified, the TI TMS320C5000 Ultra Low-Power DSP family supports USB, but not IEEE 1588 Ethernet or CAN. These interfaces could have been realized using external ICs, but in order to keep the number of electronic components to a minimum, I decided to search for a microprocessor that has integrated support for all required interfaces. This means a change of architecture, but since a significant part of the ECG system firmware is platform-independent high-level C code, porting the code is possible with reasonable effort.

In order to provide ample processing power for filtering the ECG signal, I started looking for another DSP. Among the manufacturers I considered - TI, Analog Devices and Freescale -, TI appeared to have the most detailed documentation, and they offer excellent on-line tools for microprocessor selection¹. In addition, I had already familiarized myself with their design tools, therefore I decided to choose a microprocessor by TI.

In TI's high performance DSP & ARM CPU line, I was left with two candidate families. The high-end DaVinci DSP family² has several members that offer all required communication interfaces but the capabilities of these processors far exceed the requirements of the project and they are also rather expensive. The selection tool also recommended the Sitara family³. Even though they are not DSPs, these ARM-based CPUs are aimed at performance applications and seemed to offer sufficient processing power for the ECG application at an affordable price. However, before I could order a development kit, a colleague brought TI's Concerto Microcontroller Unit (MCU) family⁴ to my attention. These microcontrollers feature all communication interfaces required by the specification, and development boards were readily available at the office.

¹ http://focus.ti.com/en/multimedia/flash/selection_tools/dsp/dsp.html

² <http://www.ti.com/lstds/ti/dsp/platform/davinci/device.page>

³ <http://www.ti.com/lstds/ti/dsp/platform/sitara/device.page>

⁴ <http://www.ti.com/mcu/docs/mcuproductcontentnp.tsp?sectionId=95&familyId=2049&tabId=2743>

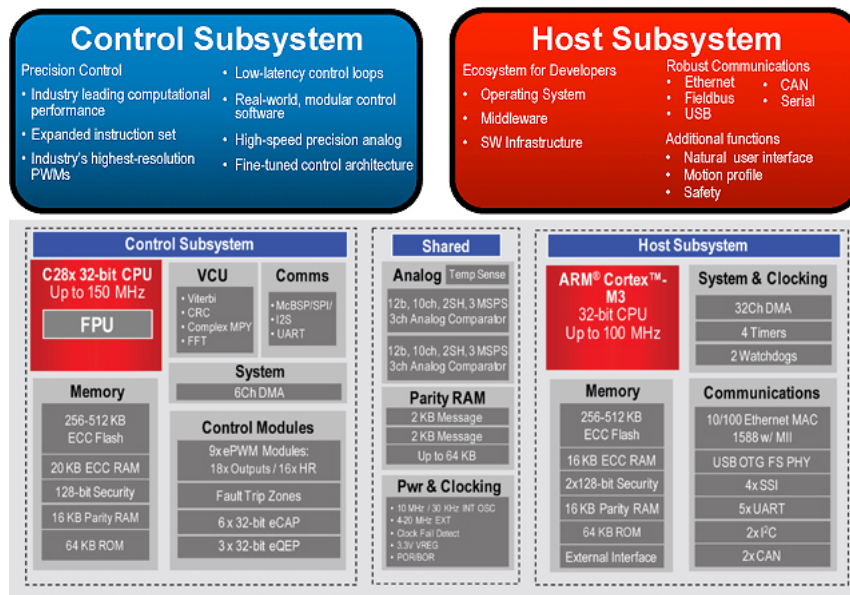


Figure 4.1: The architecture of the Concerto MCU family [17].

The Concerto family is based on a very interesting architecture, which is shown in Figure 4.1. These MCUs combine an ARM Cortex-M3 core aimed at communication with a C2000 DSP core that offers similar performance to the C5000 DSP I had used.

I carried out preliminary tests with the development board. I ported the most computationally intensive part of the firmware, the FIR filter (see Section 3.3) to the C2000 DSP core, and I also experimented with the communication between the two cores. These tests suggested that the high-end Concerto F28M35H52C1⁵ would be very suitable for the ECG system project. Since it is quite reasonably priced and also offers an integrated recyclic ADC useful for small animal respiratory measurement (see Section 4.2.4), it was chosen for hardware development.

4.2 HARDWARE DESIGN CONSIDERATIONS

Since the specification of the ECG system requires the implementation of two channels on a single board, the entire ECG hardware (see Section 4.2.3) and small animal respiratory measurement stage (see Section 4.2.4) is doubled.

Nearly all digital signal lines in the design feature series resistors for limiting transient currents.

The design features several LEDs driven by the MCU to provide a direct means of conveying information to the user.

⁵ <http://www.ti.com/product/f28m35h52c>

4.2.1 Patient protection

The IEC 60601-2-25 standard for ECGs requires that in human applications, the patient be electrically isolated from the power network and communication interfaces of the device. The breakdown voltage must be at least 4 kV.

The alternatives considered for the implementation of the isolation are the following:

- Isolation on the analog side, before the inputs of the ADS1298R.
- Isolation of the signal paths between the ECG AFE and the MCU, keeping the AFE in a separate power domain.
- Isolation of the external communication interfaces and power, keeping the MCU and the AFE in the same isolated power domain.

Creating separate, isolated power domains for each ECG AFE and isolating the digital signal paths to the MCU offers several advantages over the two other methods. Excellent methods are readily available for the isolation of on-board digital signal paths, making this alternative less cumbersome than the medical quality isolation of the communication interfaces and more robust than the isolation of analog signals. Moreover, this solution intrinsically fulfills the requirements for isolation between the two ECG stages for two patients, thus it appeared to be the best choice.

In order to provide the required isolation strengths, the portions of the board containing the ECG AFEs have been protected against leakage currents by incisions in the board layout (see Figure 4.3).

Additionally, the main power supply (see Section 4.2.2) and the CAN interfaces (see Section 4.2.6) are also electrically isolated, even though no medical quality isolation is provided in these cases.

4.2.2 Power supplies

The external components required for each regulator have been selected following the guidelines set forth in the respective datasheets. A number of ferrite bead chokes have been used throughout the design for the suppression of high frequency interference on power supply lines.

Main power supply

Since the highest supply voltage required in the ECG system is 5 V, this has been chosen as the output voltage of the main power supply. In order to comply with the requirement for a wide input voltage range and provide electrical isolation between the power network and

the board, the TEN5-2411WI DC-DC converter by TracoPower has been selected. This power supply provides a regulated output voltage of 5 V with a maximal output current of 1 A, and offers an efficiency of typically 78% [18]. Its output current is sufficient for the application, and since the sensitive components require 3.3 V power, its ripple will be suppressed by additional linear regulators.

ECG power supplies

The ECG circuitry resides in a separate power domain, which must be isolated from the rest of the board to comply with the requirements of the standard (see Section 4.2.1). In order to achieve this, the RV-0505S DC-DC converter by Recom was used. This device possesses the medical approval required by the application. With an input voltage of 5 V, it supplies a maximum output current of 400 mA at an unregulated output voltage of 5 V, with standard efficiencies of 70-75% [19].

Since the ADS1298R requires 3.3 V power and the output of the isolated power supply is unregulated, additional regulation is necessary. In order to minimize the ripple of the output voltage, linear regulation is desirable. Moreover, to suppress interference from the digital side of the IC to the analog side and thereby reduce the noise of the ADC, the best solution is having two separate regulators provide power to the analog and digital domains of the AFE. The TPS79201 by TI was chosen for its ultralow noise and high Power Supply Rejection Ratio (PSRR) [20]. Its current sourcing capabilities are largely sufficient for the requirements of the ECG stage.

CAN power supplies

The two CAN interfaces used (see Section 4.2.6) are also isolated. Their isolated power domains are supplied by TME 0505S isolated DC-DC converters from TracoPower, which provide a maximal output current of 200 mA at 5 V with an input voltage of 5 V, with a typical efficiency of 70% [21].

MCU power supply

The F28M35H52C1 MCU can operate with a single 3.3 V power supply since it has internal regulators supplying all other voltages it requires. TI's TPS79601 was selected for its excellent performance similar to the regulators used for the ADS1298R and its higher current sourcing capabilities up to 1 A [22]. Since in this case, the suppression of noise to the analog subsystem is not a critical issue, the same regulator supplies both digital and analog power, with a ferrite bead choke separating the two power domains to ensure high frequency noise reduction.

4.2.3 ECG hardware

The external components required by the ADS1298R AFE have been selected following the guidelines of the datasheet [15].

Patient protection

As discussed in Section 4.2.1, medical quality electrical isolation is required in ECG systems. In addition to placing the ECG electronics in an isolated power domain, this also requires the isolation of the digital lines to and from the AFE. Traditionally, optocouplers were used for this purpose, but this technology suffers from aging effects in the LED and difficulties at higher signaling speeds. The iCoupler technology by Analog Devices overcomes these limitations, it offers far superior performance and significantly lower power consumption [23]. The ADuM2401 device chosen for isolation offers a suitable number of input and output channels, can operate at the foreseen SPI bus frequency of 10 MHz and complies to the requirements of the IEC 60601 standard.

Since the two ECG AFEs share the same SPI bus, additional buffers gated with the respective SPI Enable signals were required on the Master In Slave Out (MISO) lines to avoid two ADuM2401 outputs concurrently driving the MISO input of the MCU.

The clock signal is routed to both AFEs from the same 2.048 MHz clock generator residing in the main power domain through the electrical isolators.

The analog input stage

The ADS1298R features a Delta-Sigma ($\Delta\Sigma$) AD converter. The $\Delta\Sigma$ modulator and the on-chip digital decimation filters can be used to filter out the noise at higher frequencies, thus the complexity of analog antialiasing filters required can be dramatically reduced with respect to Nyquist ADCs. Effectively, the input antialiasing filters are only required to filter out any interference at frequencies around multiples of f_{MOD} , the sampling frequency of the modulator [15]. In High Resolution mode, $f_{MOD} = f_{CLK}/4 = 512 \text{ kHz}$.

Therefore, only a simple RC filter is required for antialiasing at the input of the ADS1298R ICs, which was adapted from the circuit design put forward by TI in [24]. Figure 4.2 shows the magnitude response of the antialiasing filter. Complemented by the input EMI filter within the ADS1298R IC [15], this ensures the required antialiasing.

A neon lamp was added in parallel to the filter in order to provide the defibrillator protection required by the specifications on the inputs of the AFE IC. The neon lamp has a maximum strike voltage of 90 V [25]. In conjunction with the resistor in series, it limits transient

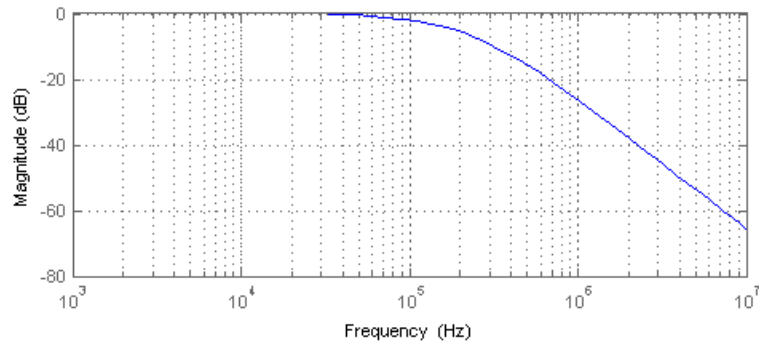


Figure 4.2: Frequency response of the input antialiasing filter. The graph confirms that, together with the EMI filter within the ADS1298R, the filter ensures the antialiasing required.

currents reaching the inputs of the ADS1298R to approximately 9 mA, which the inputs can withstand [15].

4.2.4 Small animal respiratory measurement

Based on previous experience, the SDP1108-R differential pressure sensor by Sensirion has been chosen for the purpose of respiratory measurement. It requires a 5 V DC power supply and provides a fully calibrated analog voltage output. It offers a full scale pressure difference of 500 Pa with superior accuracy, outstanding resolution and low temperature dependence through internal compensation [26].

The proposed measurement configuration consists of a tiny respiration sensor cushion⁶ the small animal lies on for measurement. The output of the cushion is connected to the Hi terminal of the SDP1108-R, while the Lo terminal is left open, thus atmospheric pressure is used as reference. The performance of the SDP1108-R makes it highly suitable for measuring the small volume flows generated by the cushion through the breathing of the animal.

The analog output voltage of the SDP1108-R is connected to an ADC input of the MCU for digitization. Since the output voltages range from 0.25 V to 4 V and the ADC operates with a reference voltage of 3 V, a voltage divider is required between the output and the input. In addition, an optional RC filter has been added to the design to ensure the possibility of limiting high-frequency noise.

⁶ E.g. <http://www.medicare.ie/mother-baby/infant-respiration-monitors-rental-1/graseby-respiration-sensor.html>.

4.2.5 *Microcontroller unit*

The quartz oscillator, decoupling capacitors, pullup/pulldown resistors and other required external components have been laid out according to the guidelines of the datasheet [27].

A JTAG interface has been implemented for programming and debugging.

The F28M35H52C1 offers a total of five SPI interfaces. Both ECG AFEs are connected to the only one of those that is controlled by the DSP core to allow for readout and data processing by the same core.

In addition to the output of the pressure sensors (see Section 4.2.4), two supply voltages have been connected to ADC inputs of the Concerto through resistive dividers to allow monitoring the state of the power supplies.

4.2.6 *Communication interfaces*

Ethernet

In addition to the Ethernet MAC in the Concerto, a transceiver IC and an RJ-45 connector is required for Ethernet communication. This circuitry has been adapted from the circuit design of the TI H52C1 Concerto ControlCard [28].

USB

The F28M35H52C1 includes the implementation of the physical layer, therefore only a USB connector is required for communication. Since the ECG system is only meant to be used as a USB device, a simple USB-B connector has been implemented in the design, along with protection diodes on the data lines.

CAN

The ECG system design makes use of both CAN interfaces of the Concerto. CAN is used as an external communication interface and also for connecting to the slave modules (see Chapter 2). 9-pin D-SUB male connectors are used.

To complement the isolated power supplies, TI's ISO1050 isolated CAN transceivers [29] have been used in the design for CAN interface isolation.

In addition to protection diodes on the CAN data lines, the slave module ("bed") CAN circuitry features a solution that disables the local CAN termination resistor if the slave modules for both channels are attached. In contrast, the external CAN interface complies to the protocol in use at Mediso, thus it features a termination resistor that can be enabled externally through the D-SUB connector.

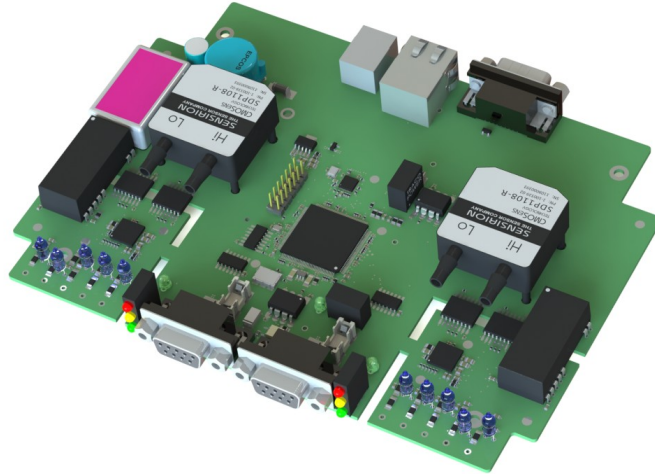


Figure 4.3: Rendered visualization of the populated ECG printed circuit board. Note the incisions protecting the ECG circuitry from leakage currents.

4.3 THE HARDWARE

Based on the aforementioned considerations, the schematic (see [Appendix A](#)) and layout design of the final printed circuit board have been completed. At the time of writing this thesis, the circuit board is being manufactured. [Figure 4.3](#) shows a rendered visualization of the populated printed circuit board.

MEASUREMENTS

Since no final ECG system hardware has been produced yet at the time of writing this thesis, all measurements described in this chapter were carried out using the ECG prototype system. However, the expected performance of the final hardware is very similar.

The output of the ECG system has not yet been calibrated for converting output values to voltages, thus all amplitude axes show values in arbitrary units.

5.1 ECG SIGNAL ACQUISITION

5.1.1 ECG simulator

Initial ECG measurements were made with an ECG simulator, a device featuring connectors for ECG lead wires and capable of generating ECG waveforms. The ECG system was connected to the simulator with a standard human ECG cable in a 5-electrode configuration, as shown in Figure 3.3. The following examples illustrate the performance of the system with input signals from the simulator.

Figure 5.1 shows a recording of the ECG simulator output with amplitude set to 1 mV and heart rate set to 60 bpm. The unfiltered ECG data features very characteristic P and T waves and QRS complex, along with a negligible contribution from power line interference. In this case, the unfiltered data would be directly usable for QRS detection, however, filtering was carried out for comparison. Since the bandpass filter for human applications was used, use of the notch filter for power line interference suppression was not required.

Suppression of the DC component by the baseline restoration filter is well visible in the filtered data. The limited delay and waveform distortion resulting from the FIR filter are also identifiable, however, these effects are acceptable (see Section 3.3.2). As a result, the discrete derivative provides a perfectly usable QRS metric.

Figure 5.2 depicts a recording of the output of the simulator with the same settings (note the different scale on the time axis), deliberately corrupted by 50 Hz power line noise by placing a soldering iron close to the ECG system. The filtering does a remarkable job in eliminating power line interference and a usable QRS metric is produced.

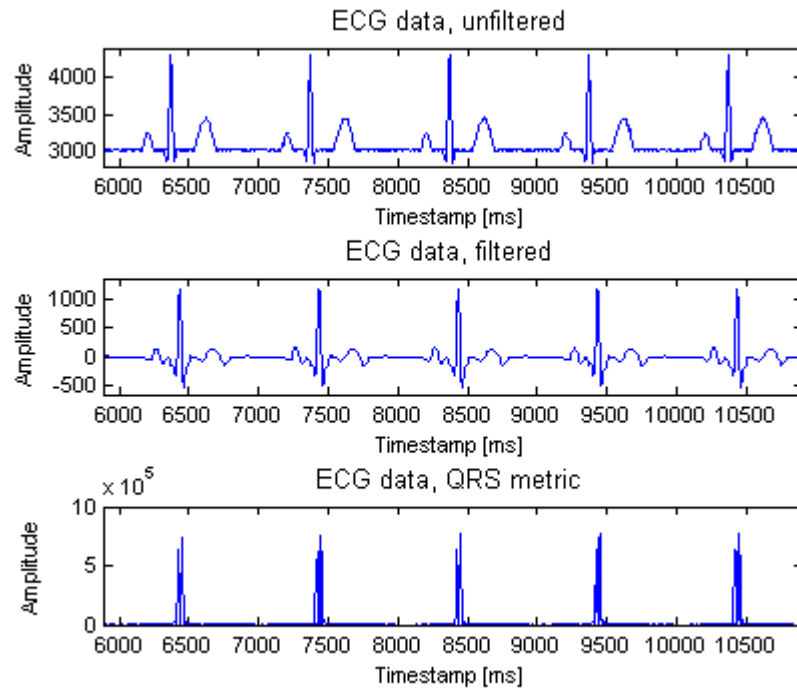


Figure 5.1: Recording of the ECG simulator output.

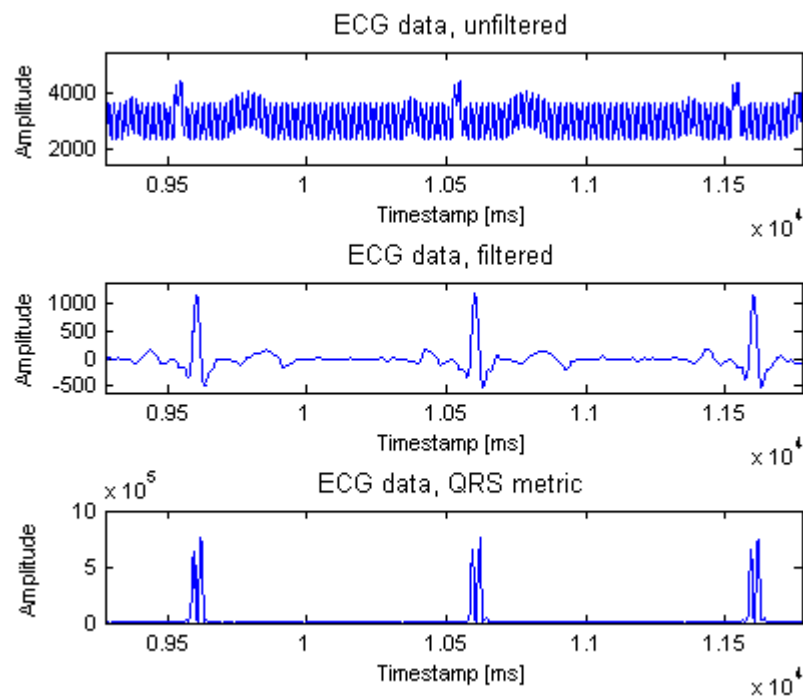


Figure 5.2: Recording of the ECG simulator output, corrupted by 50Hz noise. This figure demonstrates the efficiency of the notch filter in eliminating power line interference.

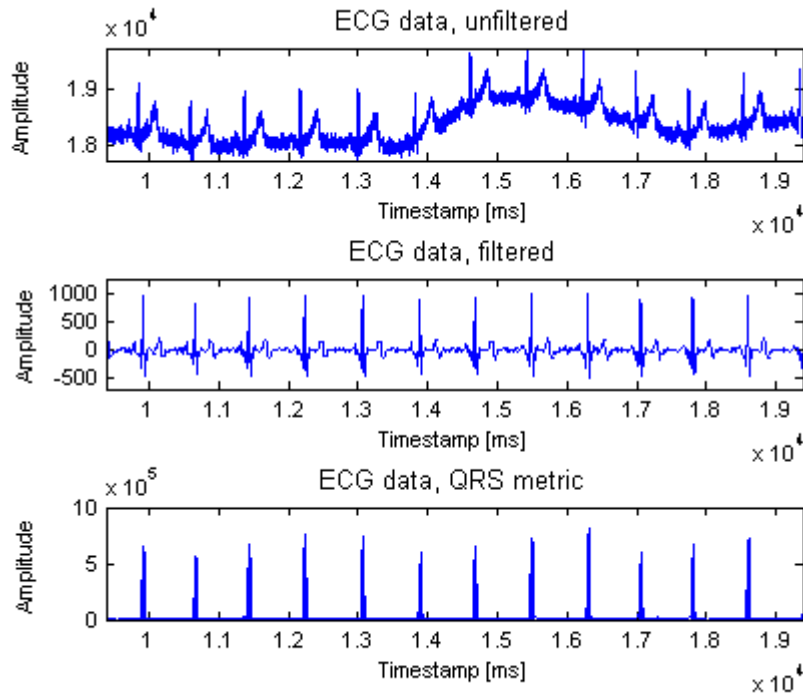


Figure 5.3: Human ECG recording. This figure illustrates the power of the filters in suppressing power line interference and baseline wander.

5.1.2 Human ECG

Figure 5.3 shows the author's ECG recording at rest, acquired in a 3-electrode configuration with LA and RA input electrodes, and the RL feedback electrode connected to the appropriate limbs. The recording exhibits noticeable power line interference and breathing causes significant baseline wander in the ECG trace. However, these distortions are eliminated by the DC suppression and bandpass filters. This yields a very high quality metric for QRS detection. The average heart rate during the measurement can be identified as approximately 75-80 bpm.

Figure 5.4 shows the author's stress ECG recording while performing squats. The baseline restoration filter performs remarkably once more, however, due to muscle movement, the unfiltered ECG data exhibits sharp transitions the currently used filters cannot eliminate satisfactorily. This leads to the presence of spurious pulses in the QRS metric, thus unwanted QRS triggers.

5.1.3 Small animal ECG

To verify its capability to acquire the ECG signals of rodents, the ECG system was tested with anesthetized small animals. These recordings

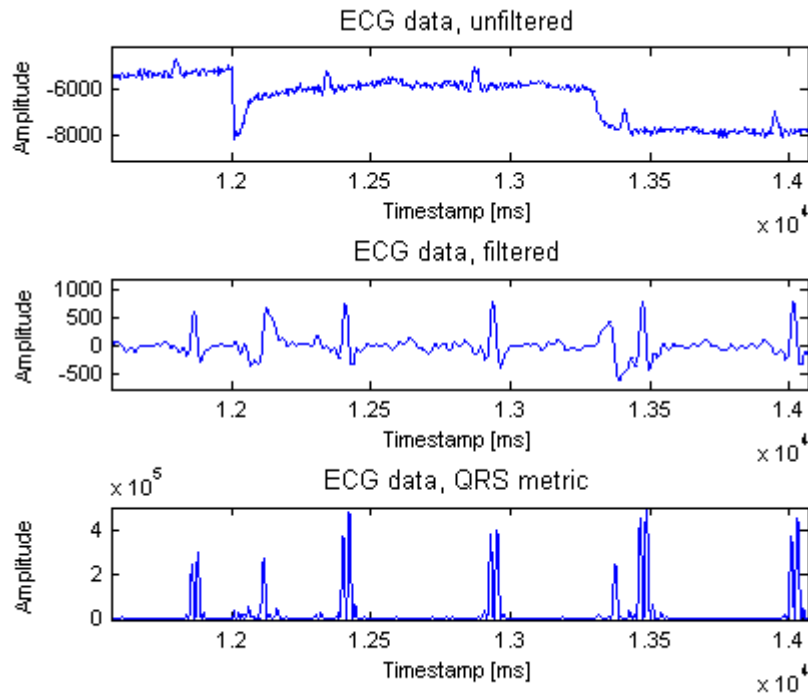


Figure 5.4: Human stress ECG recording. This figure demonstrates the challenges faced in the processing of stress ECG signals.

were carried out in a 3-electrode ECG configuration with LA and RA input electrodes and a feedback electrode, RL, connected to the limbs of the animal. 3M Red Dot neonatal, pre-wired, radiolucent monitoring electrodes were employed with a standard, unshielded ECG cable. The bandpass filter for small animal measurements was used, therefore the notch filter for power line interference was required (see Section 3.3.2).

The photo of an anesthetized rat fitted with ECG electrodes can be seen in Figure 5.5. Figure 5.6 shows the ECG signal recording. The unfiltered signal suffers from significant power line interference. Due to the transients of the notch filter, this interference is only attenuated, not completely eliminated. Filtering also reduces the amplitudes of the QRS complexes. However, both the unfiltered and the filtered signal yield a usable QRS metric through the discrete derivative filter. The heart rate of the rat was measured to be around 235 bpm (see Figure 3.7), which is in accord with the values found in the literature [30].

Figure 5.7 shows the ECG of a hamster. Surprisingly, the signal features inverted QRS complexes due to biological reasons. The signal exhibits limited baseline wander and negligible power line interference. In this case, filtering yields no obvious improvement with respect to the unfiltered signal, and the amplitudes of the QRS complexes are re-

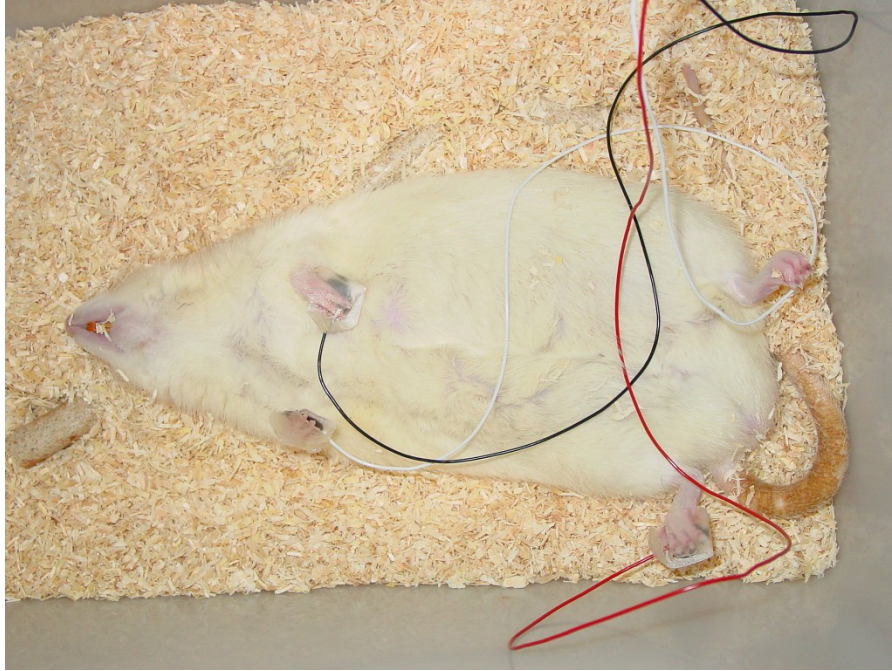


Figure 5.5: The anesthetized rat fitted with ECG electrodes.

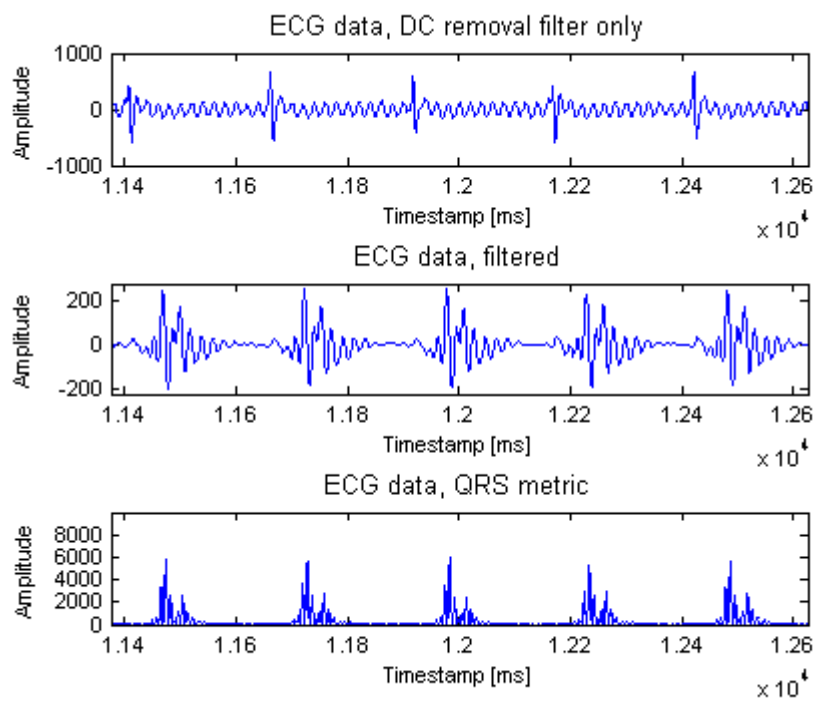


Figure 5.6: Rat ECG recording. This figure illustrates the capability of the processing to create a usable QRS metric.

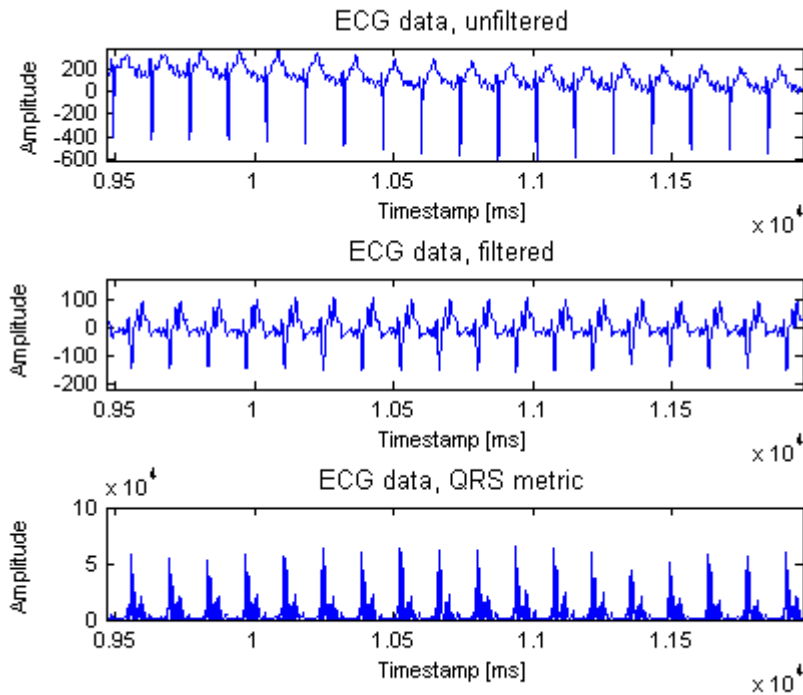


Figure 5.7: Hamster ECG recording. This figure demonstrates the ability of the processing to create a usable QRS metric.

duced. However, as was the case with the ECG of the rat, both filtered and unfiltered signals are usable for QRS detection. The heart rate of the hamster was measured to be around 430 bpm, which corresponds to the values found in the literature [31].

5.2 PERFORMANCE IN MRI

Mediso assembles permanent magnet MRI machines for small animal applications. Compared to electromagnet-based devices, these machines offer the advantage of a limited fringe field [32], thus metallic objects may be brought into the vicinity and ordinary electronic devices may be operated near the machine. This means that ECG measurement in MRI might be possible by setting up the ECG system next to the MRI machine and using MRI-compatible ECG electrodes within the bore of the MRI magnet.

The manufacturer claims that the 3M electrodes I used for small animal ECG measurements (see Section 5.1.3) are not MRI-compatible. Nevertheless, the electrodes are non-ferrous and the pre-attached lead wires are made of carbon. Moreover, Small Animal Instruments, Inc. use the same electrodes in their MRI-compatible ECG system [10], thus these electrodes were good candidates for measurements in MRI.

5.2.1 Initial measurements

In order to assess the viability of measuring ECG as outlined above, I carried out initial measurements with an MRI water phantom and the 3M electrodes within the magnet bore. The two ECG electrodes that form the ECG lead under measurement were connected together with approximately 100 k Ω contact impedance, which reasonably approximates usual ECG contact impedances. This setup was placed in the MRI animal bed underneath the phantom and inserted into the MRI bore. No actual signal source was connected to the electrodes, thus the measurement was expected to register background noise and eventual MRI contributions.

Figure 5.8 shows the result of the acquisitions. The upper plot depicts the spectrum of the background acquired within the MRI bore, with no MRI sequence in progress. The spectrum is clearly dominated by 50 Hz power line interference with significant harmonic content. The lower plot shows the spectrum of the data acquired during the execution of a scout MRI sequence. I deemed the results promising, since MRI contributions are only visible around 260 Hz and 480 Hz, outside of the frequency band of interest, and should therefore be easy to attenuate. It is noteworthy that 260 Hz corresponds to the repeat period of the radio frequency pulses in the scout sequence, 3.8 ms. It should also be noted that although the spectra of the 50 Hz harmonics are visually similar, MRI interference appears to amplify several harmonics.

The MRI images acquired of the phantom with the electrodes in place were only slightly deteriorated, showing limited signs of interference generated by the electrodes. The electrodes were not visible on the MRI image.

5.2.2 Small animal measurements

ECG measurements

Based on the positive experience gained with the initial measurements, I attempted measuring the ECG of a hamster within MRI. I used the same electrode configuration as in Section 5.1.3. Measurements with the hamster inside the MRI bore, but with the gradient and radio frequency systems of the MRI machine turned off, yielded results in excellent agreement with those obtained outside of the machine. Thus, the field of the permanent magnet appears to have no noticeable influence on the measurement.

Figure 5.9 shows the result of the measurements. The upper plot depicts the spectrum of the hamster ECG acquired within the MRI bore, with no MRI sequence in progress. It is interesting to note that the spectrum appears to be discrete, which suggests that the heart rate of the hamster is very steady. The lower plot shows the spectrum of

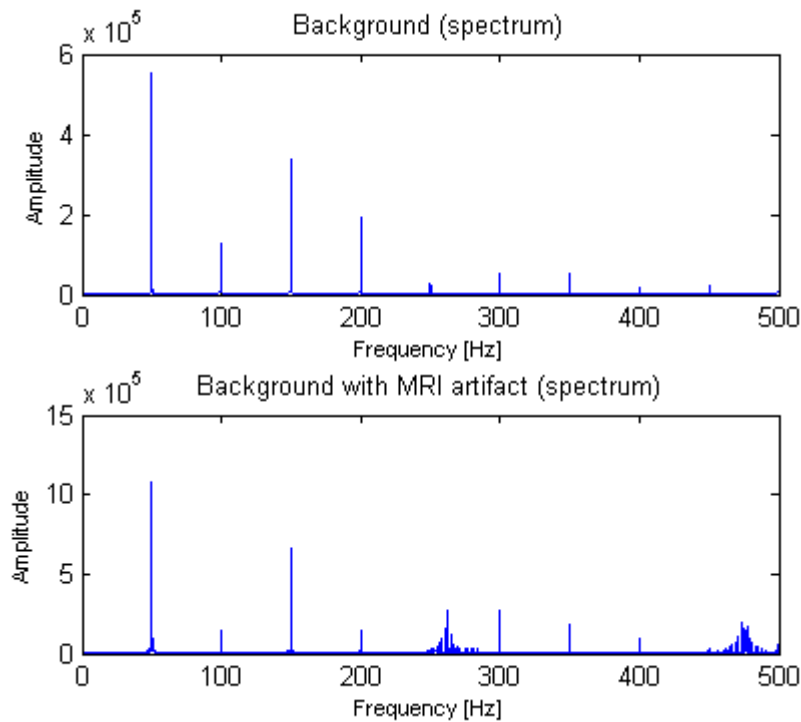


Figure 5.8: Spectrum of the background signal acquired within the MRI bore, without MRI sequence in progress and during a scout sequence.

the data acquired during the execution of a scout MRI sequence. MRI interference appears at the same frequencies that were identified earlier, however, in this case, it dominates the signal. This demonstrates a weakness of the filtering in use: Figure 5.10 shows that the low frequency spectrum of the hamster ECG is partially preserved, with some frequency components diminished. However, the filtering cannot sufficiently attenuate the high-frequency interference, thus QRS detection on the filtered signal fails.

Figure 5.11 shows an ECG spectrum acquired during execution of a spin echo MRI sequence. The high frequency components of the spectrum were attenuated by the small animal band-pass filter. This MRI sequence appears to cause a wide-band interference within the frequency band relevant for ECG acquisition, along with some very high peaks. QRS detection on this signal yields no usable results.

MRI measurements

In contrast to the phantom measurements described in Section 5.2.1, no usable MRI images of the hamster fitted with ECG electrodes could be acquired with the sequences tested.

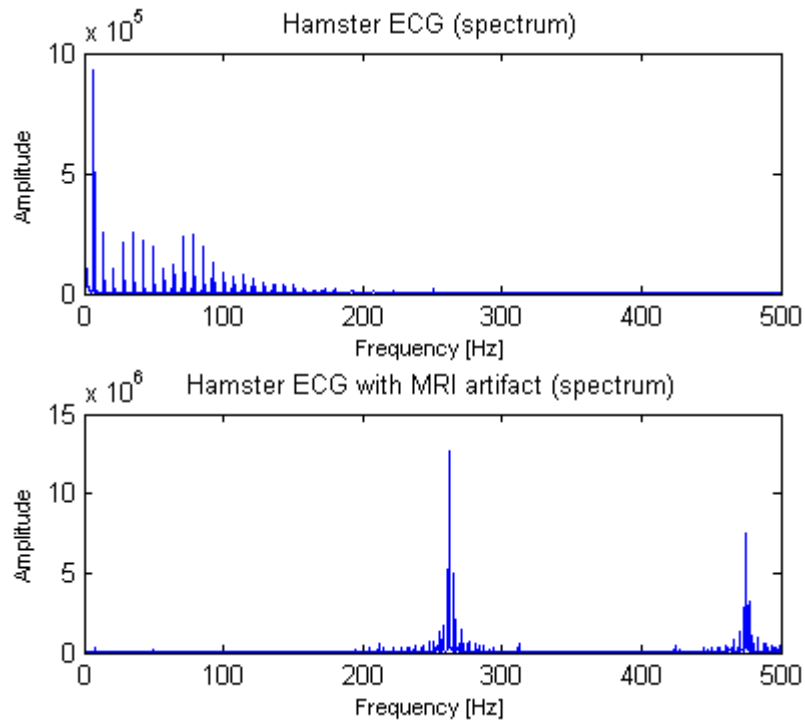


Figure 5.9: Spectrum of a hamster ECG acquired within the MRI bore. During the scout sequence, MRI artifact dominates the spectrum.

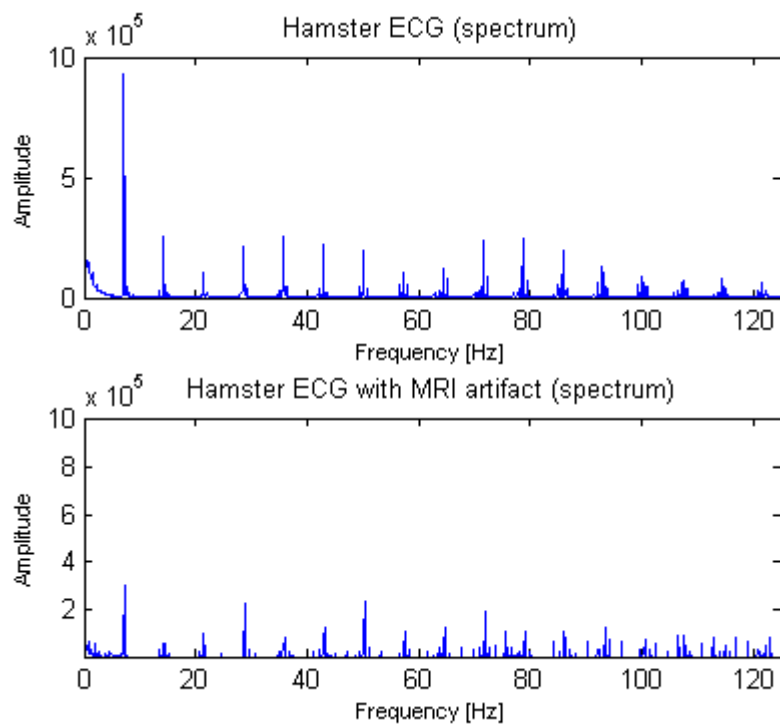


Figure 5.10: Spectrum of a hamster ECG acquired within the MRI bore, zoomed in. The spectrum has been partially preserved at low frequencies, even despite MRI artifact from the scout sequence.

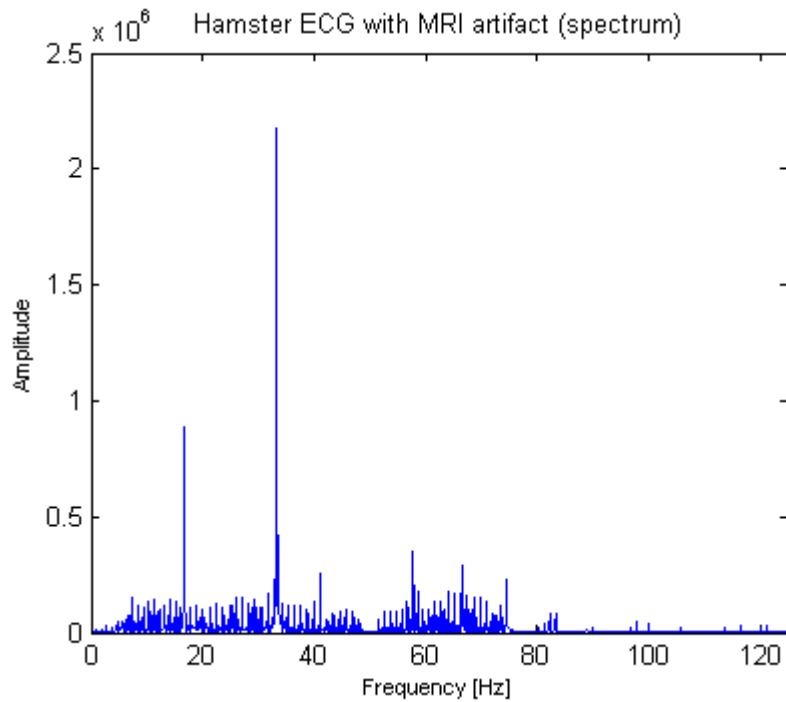


Figure 5.11: Spectrum of a hamster ECG acquired within the MRI bore during a spin echo sequence. The high frequency components were attenuated by the small animal band-pass filter.

5.2.3 Discussion

At present, the interactions between the ECG system and the MRI machine impair both ECG signal acquisition and MRI image creation.

MRI image creation

The comparison of MRI images acquired of the phantom and of the hamster, both in presence and absence of ECG electrodes, shows a degradation in the quality of the MRI images when the electrodes are present. The images suggest that this effect is due to radio-frequency interference caused by the presence of the ECG electrodes in the MRI bore, which probably act as antennas in guiding interference into the MRI acquisition volume. However, the degradation is much more significant in the case of hamster measurements, where it yields unusable images, whereas for phantom measurements, it merely causes grainy artifacts but image quality remains acceptable. This implies that the body of the animal amplifies the radio-frequency interference guided into the MRI volume by the electrodes.

Nonetheless, in the case of phantom measurements, the ECG electrodes were connected together with a contact impedance (see Section 5.2.1), while in the case of hamster measurements, they were connected to the limbs of the animal (see Section 5.2.2). In order to

evaluate the role of the animal body in the amplification of the interference, phantom measurements should be carried out in a similar configuration, ensuring that the electrodes are physically separated. Since the phantom is made of plastic and is thus probably an insulator, appropriate contact impedances must be ensured between the different electrodes. Due to the limited amount of time available after the first animal MRI experiments, this measurement has not been carried out yet.

Colleagues with MRI-related experience suggested adding 1 nF filtering capacitors between all ECG electrode lines and the common ground to reduce radio-frequency interference, but our measurements carried out with the phantom showed no quantifiable improvement nevertheless.

ECG acquisition

A tentative simulation showed that by applying a band-pass filter with sufficient attenuation in the higher stopband to the ECG signal corrupted by interference from the scout sequence, the remaining low-frequency components (see Figure 5.10) can be used to produce an almost usable QRS metric. This implies that in the case of this sequence, further tweaking of the already implemented digital filtering could probably be used to satisfactorily eliminate MRI interference from the ECG signal.

However, several other sequences that were tested, e.g. spin echo, produce wide-band interference within the frequency band of interest for ECG measurement (see Figure 5.11). In these cases, the filtering used in the ECG prototype system gives little hope of eliminating MRI interference, thus new filtering techniques need to be considered. Since the stray magnetic field of the solenoidal radio-frequency excitation coil of the MRI machine can be expected to be small, and as discussed in Section 4.2.3, the inputs of the ECG AFE are equipped with sufficient analog filtering against out-of-band interference, digital filtering will probably be appropriate.

Measurements also revealed that the position of the ECG cable has a great influence on the sensitivity of the system to power line interference. Further investigations could help establishing good practices of cable layout.

SUMMARY

6.1 ACCOMPLISHMENTS

I spent the past year working at Mediso Medical Imaging Systems. During this time, based on two different development kits, I produced an ECG prototype system, which is fully functional with the firmware I designed. I demonstrated the ability of the system to acquire human and small animal ECG waveforms and detect QRS complexes.

Based on the experience gained with the prototype system, we designed the final ECG system board. The circuit board is being manufactured at the time of writing this thesis. Utilizing my work done for the prototype and a demonstration board, I have completed the development of a great part of the firmware of the future ECG system.

6.2 POSSIBILITIES OF IMPROVEMENT

The measurements carried out so far show that the system is not yet able to perform satisfactorily in the MRI environment. The interactions of the ECG system with MRI require further investigation in order to achieve MRI-compatibility.

The firmware developed for the final ECG system needs to be completed and it should be tested with the final board as soon as the latter is available.

The filters in use should be reviewed in order to eliminate the glitches encountered during the acquisition of human stress ECG.

The ECG output amplitudes need to be calibrated in order to allow voltage readout, taking into consideration the amplification of the band-pass filters.

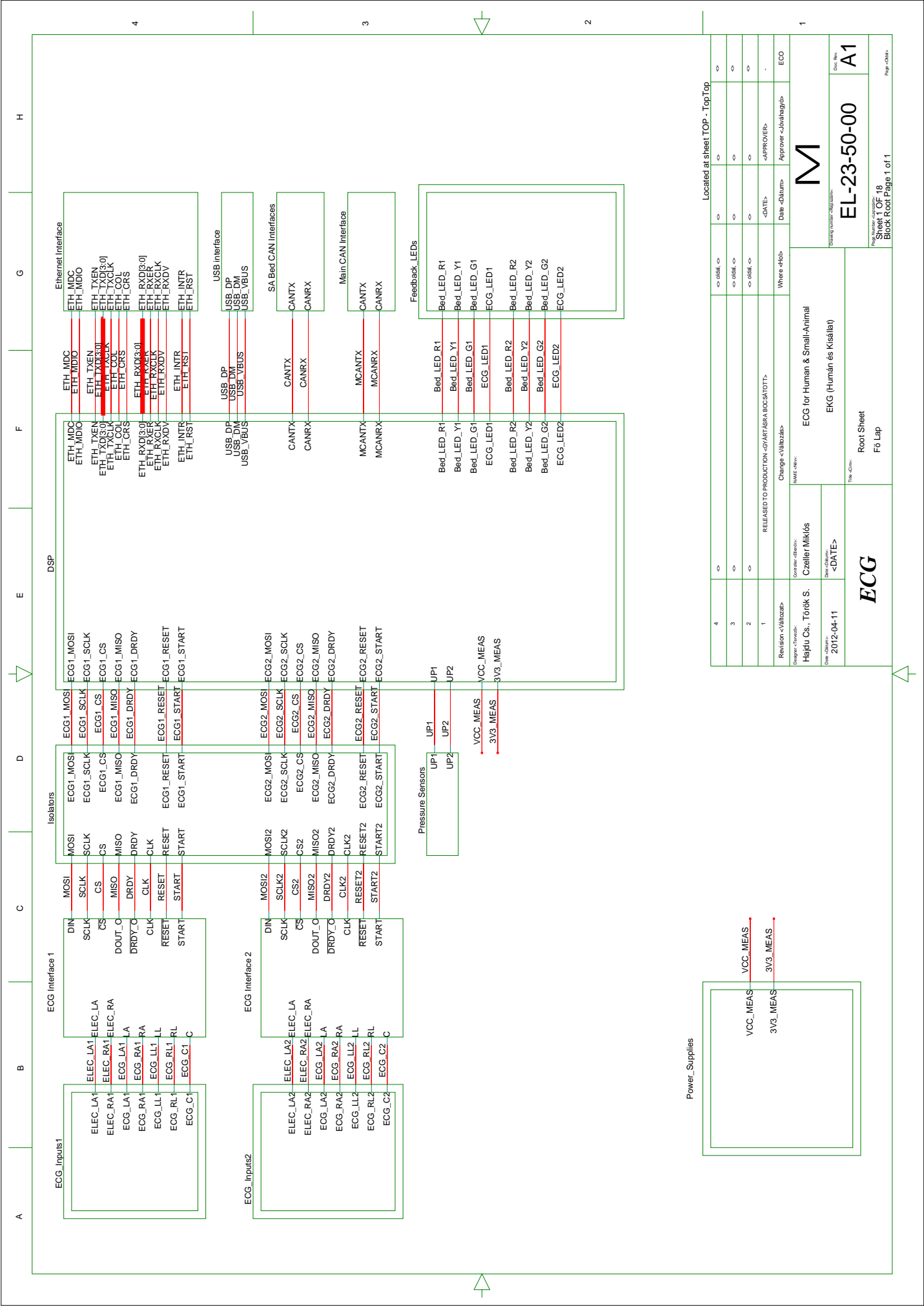
By keeping the currently used filters for QRS detection, and implementing another set of filters which satisfactorily preserve all key features of the ECG waveform for display, a diagnostic quality ECG could probably be produced.



APPENDIX

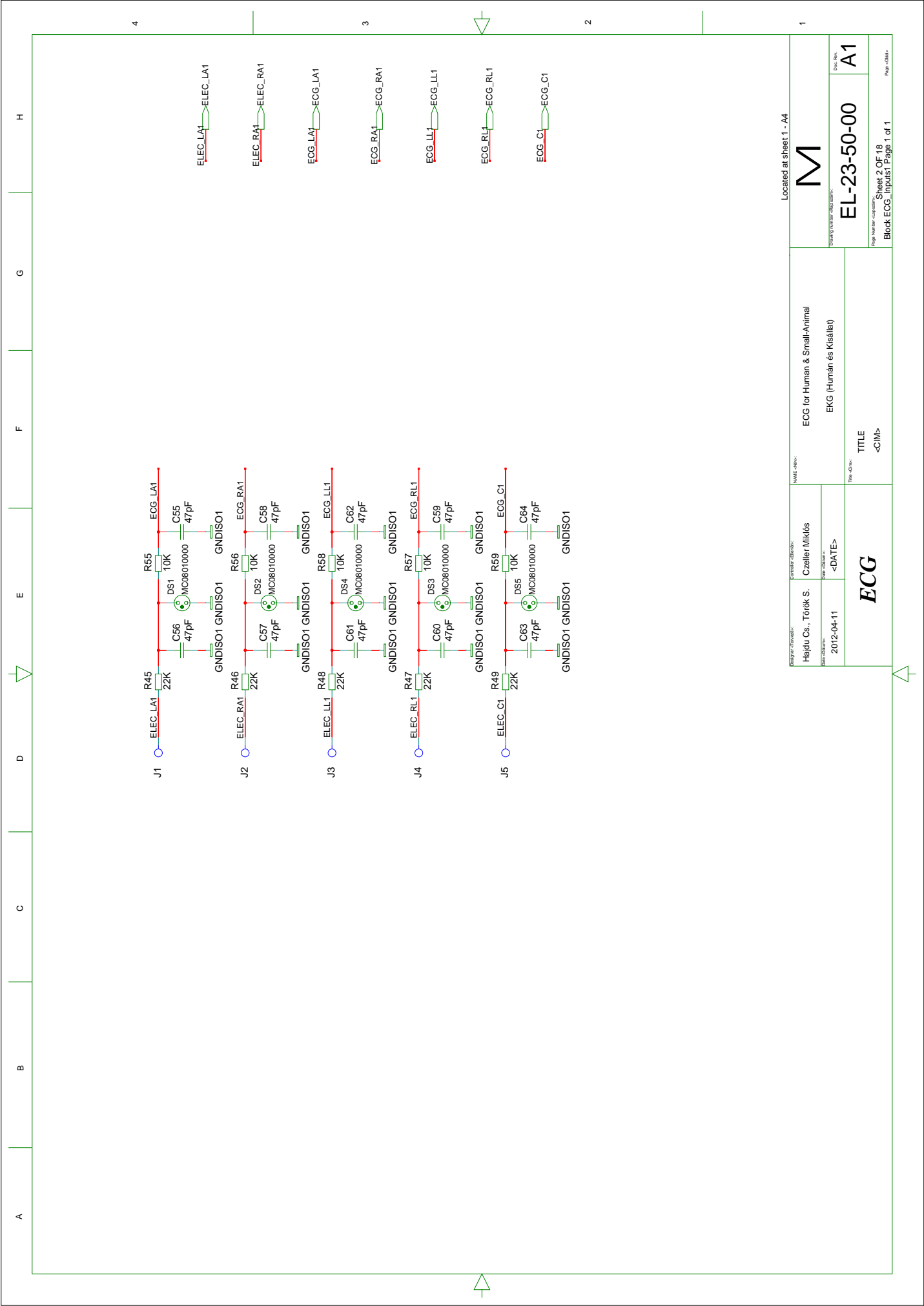
Listing A.1: Configuration of the ADS1298R.

```
// ADS1298R register values
Uint8  ADS1298RegVal[25] = {
#if  ECG_SAMPLERATE == 500
    0x86, // Register CONFIG1: Hi-Res EN, data rate = 500SPS
#elif ECG_SAMPLERATE == 1000
    0x85, // Register CONFIG1: Hi-Res EN, data rate = 1000SPS
#elif ECG_SAMPLERATE == 2000
    0x84, // Register CONFIG1: Hi-Res EN, data rate = 2000SPS
#elif ECG_SAMPLERATE == 4000
    0x83, // Register CONFIG1: Hi-Res EN, data rate = 4000SPS
#else
    #error Sample rate not supported!
#endif
    0x10, // Register CONFIG2: variable WCT chopping frequency
    0xDD, // Register CONFIG3: RLD buffer EN; Vref = 2.4V
    0x03, // Register LOFF: DC current source Loff detection
    0x00, // Register CH1SET: normal operation, PGA gain = 6
    0x00, // Register CH2SET: id.
    0x00, // Register CH3SET: id.
    0x00, // Register CH4SET: id.
    0x00, // Register CH5SET: id.
    0x00, // Register CH6SET: id.
    0x00, // Register CH7SET: id.
    0x00, // Register CH8SET: id.
    0x06, // Register RLD_SENSP: channels 2 and 3 (LA, LL) in RLD
    0x02, // Register RLD_SENSN: channel 2 (RA) in RLD
    0xFE, // Register LOFF_SENSP: Loff EN on all chans but IN1P
    0x02, // Register LOFF_SENSN: Loff EN on IN2N (RA)
    0x00, // Register LOFF_FLIP: Loff curr direction: default
    0x00, // Register LOFF_STATP (read only)
    0x00, // Register LOFF_STATN (read only)
    0x0F, // Register GPIO: all GPIOs set to input (unused)
    0x00, // Register PACE: PACE detect buffer off
    0xF0, // Register RESP: respiration switched off
    0x22, // Register CONFIG4: Loff comparators powered up
    0x0A, // Register WCT1: IN2P (LA) -> WCTA
    0xE3, // Register WCT2: IN3P (LL) -> WCTB, IN2N (RA) -> WCTC
};
```



Located at sheet: TOP - TopTop

4	<	>	<	>	<	>	<	>	<	>
3	<	>	<	>	<	>	<	>	<	>
2	<	>	<	>	<	>	<	>	<	>
1	<	>	<	>	<	>	<	>	<	>
Revision: <Működés> Released to production: <GYÁRTÁSRA Bocsátott> Where: <Hely>										ECO
Designer: <Művezető> Name: <Név> ECG for Human & Small-Animal										M
Draw: <Ábrát készítő> Date: <Dátum> 2012-04-11										
ECG (Humán és Kisállat)										Doc. No.:
Root Sheet Fő Lap										EL-23-50-00
ECG										Sheet 1 OF 18
Fő Lap										Page: <Oldal>



A B C D E F G H

4

3

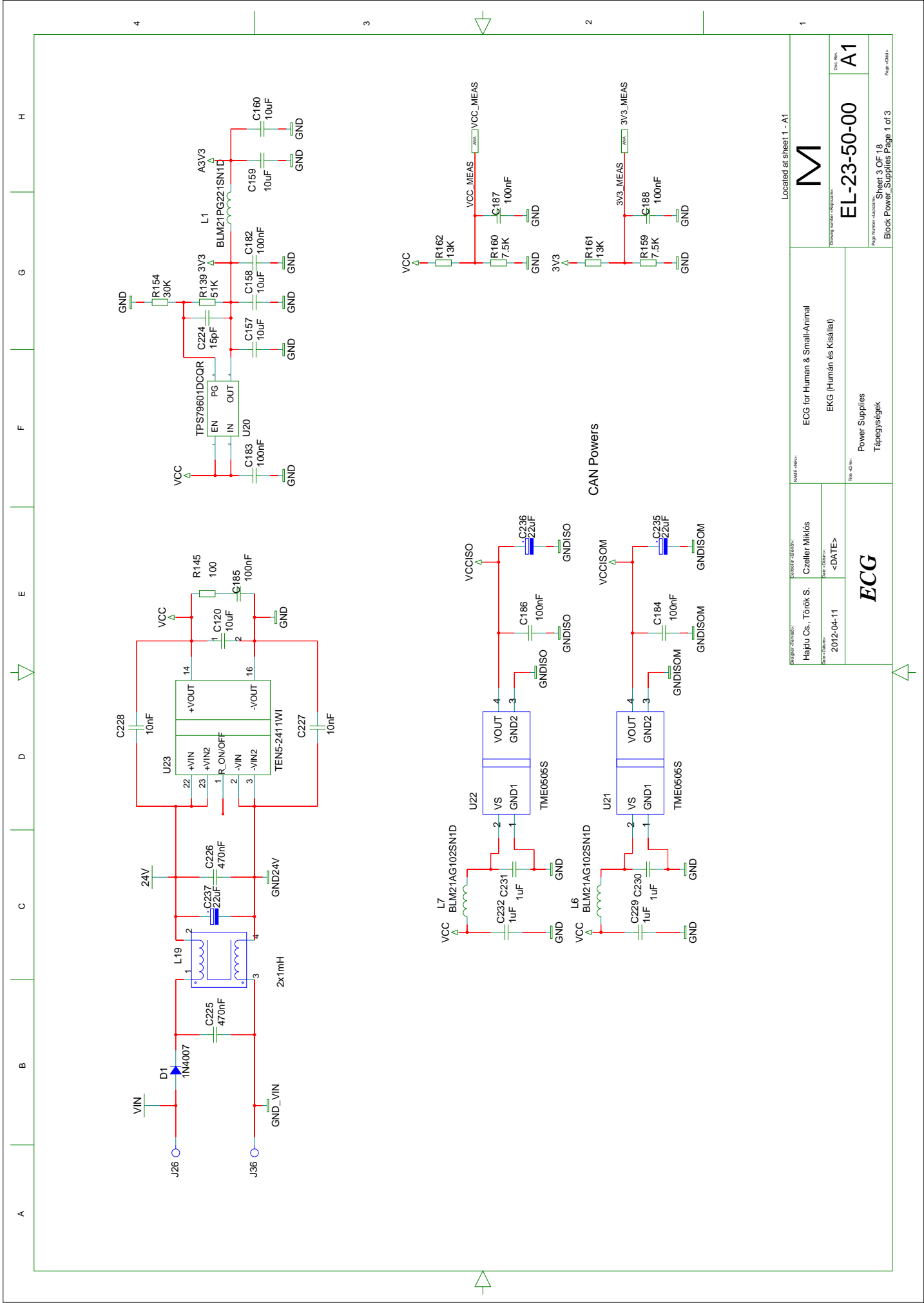
2

1

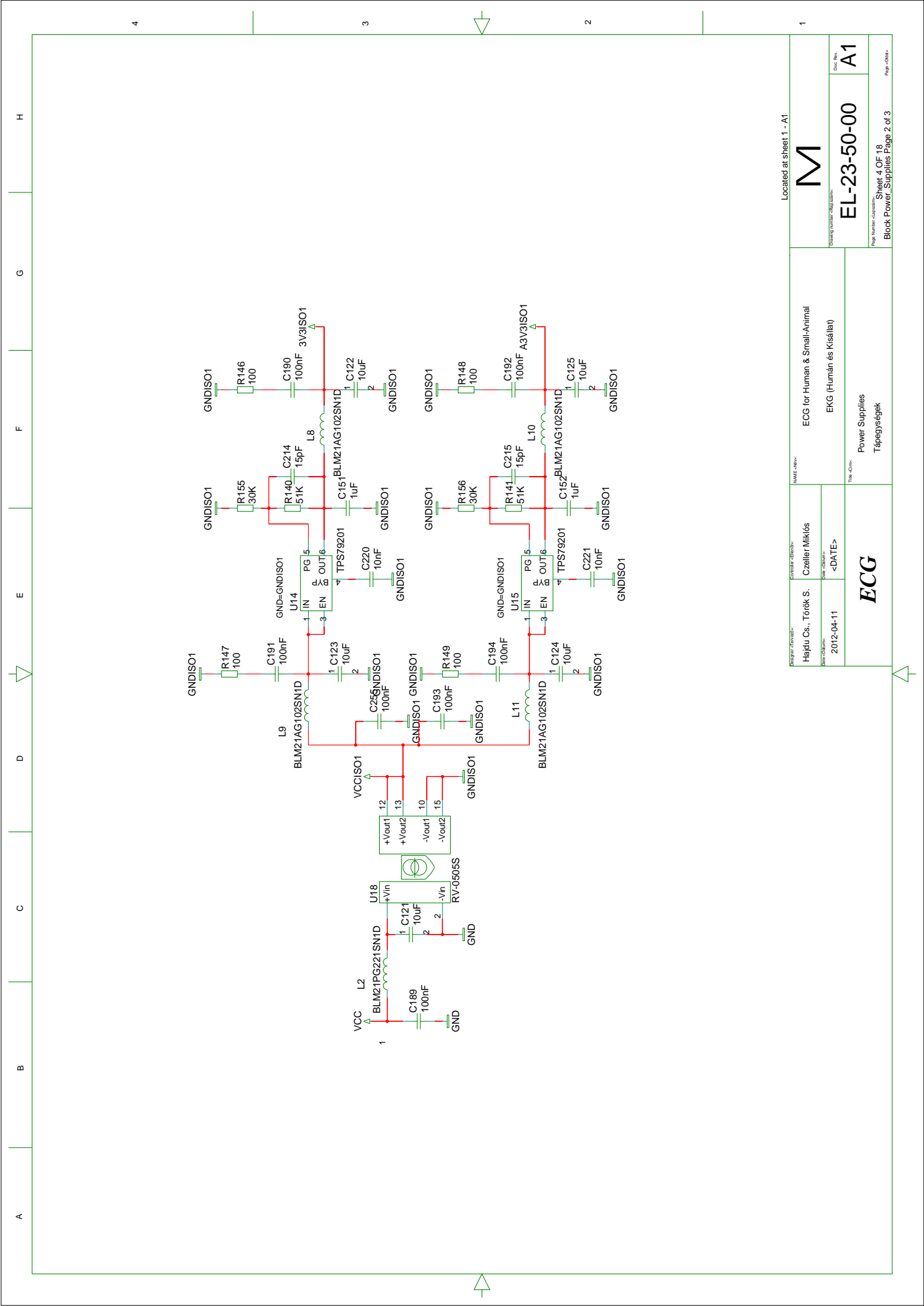
Located at Sheet 1 - A4

Program: HELYDAS Designer: Czeller Miklós Date: 2012-04-11		Name: ECG for Human & Small-Animal Description: EKG (Humán és Kisállat)		 EL-23-50-00 Drawing number: EL-23-50-00 Page number: Sheet 2 of 18 Block: ECG Input1 Page: 1 of 1
Title: ECG		Title: <CIM>		

A1



Program: HEJDU Designer: Török S. Date: 2012-04-11		Project: ECG Designer: Czeller Miklós Date: <DATE>		Name: ECG for Human & Small-Animal Part: EKG (Humán és Kisállat)		Drawing number: EL-23-50-00 Page number: Sheet 3 OF 18 Page count: Block Power_Supplies Page 1 of 3	
ECG				Power Supplies Tápegységek			
Located at Sheet 1 - A1							



A B C D E F G H

1 2 3 4

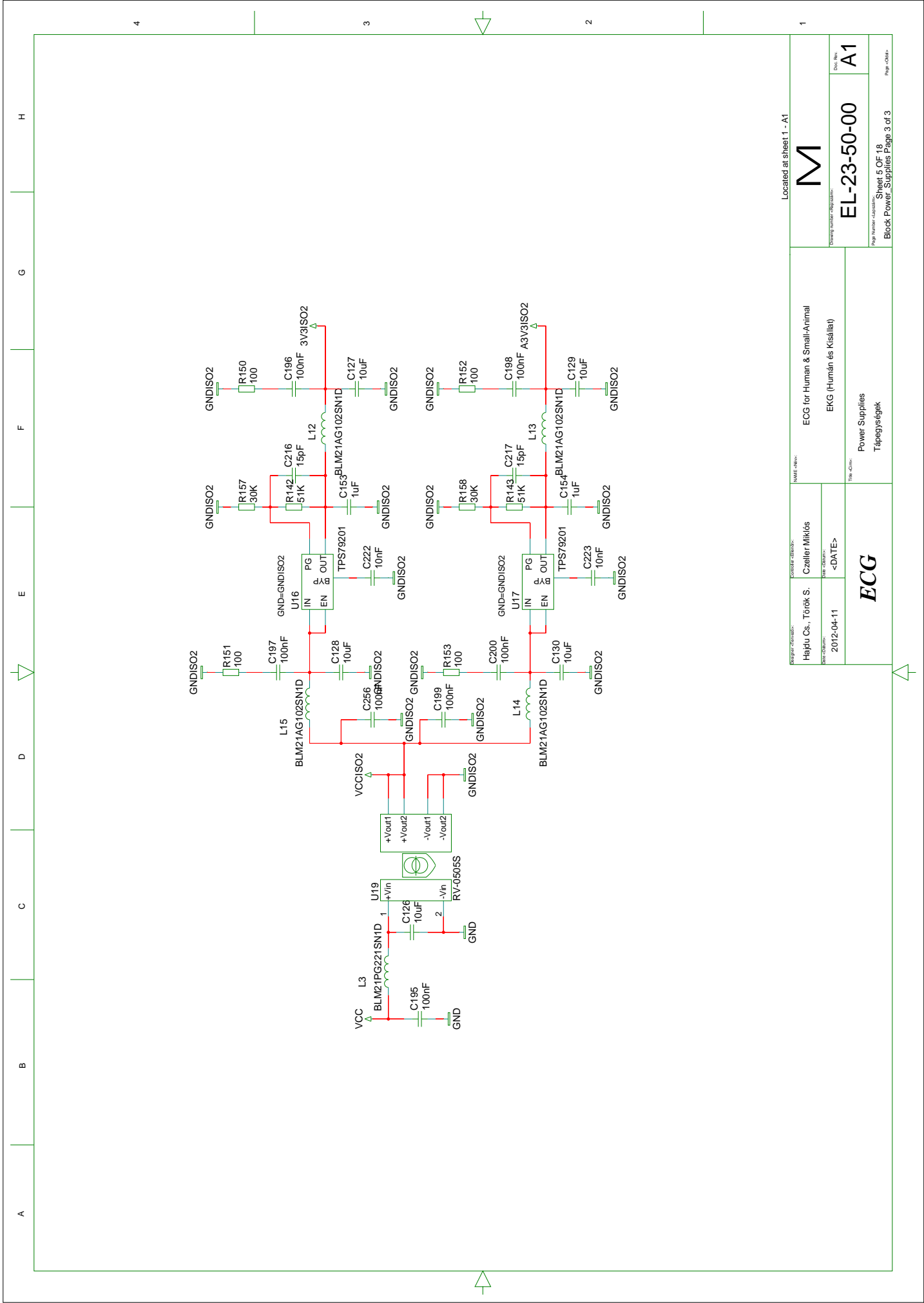
M	Doc. No. A1
EL-23-50-00	Page Number / Total Pages Sheet 4 OF 18
Block Power Supplies	Page Number / Total Pages Block Power Supplies Page 2 of 3

Located at Sheet 1 - A1

<p>Project Name: ECG for Human & Small Animal</p> <p>Customer Name: ECG (Humán és Kisállat)</p>	<p>Project Name: ECG</p> <p>Customer Name: ECG (Humán és Kisállat)</p> <p>Project Manager: Tápegységek</p>
---	---

<p>Project Manager: Hejdu Cs., Török S., Czeller Miklós</p> <p>Start Date: 2012-04-11</p>	<p>Project Name: ECG</p> <p>Customer Name: ECG (Humán és Kisállat)</p> <p>Project Manager: Tápegységek</p>
---	---

<p>Project Name: ECG</p> <p>Customer Name: ECG (Humán és Kisállat)</p> <p>Project Manager: Tápegységek</p>	<p>Project Name: ECG</p> <p>Customer Name: ECG (Humán és Kisállat)</p> <p>Project Manager: Tápegységek</p>
---	---



H

G

F

E

D

C

B

A

4

3

2

1

Located at Sheet 1 - A1



Doc No:	A1
Part Number:	EL-23-50-00
Page Number:	Sheet 5 OF 18
Page Count:	Block Power Supplies Page 3 of 3

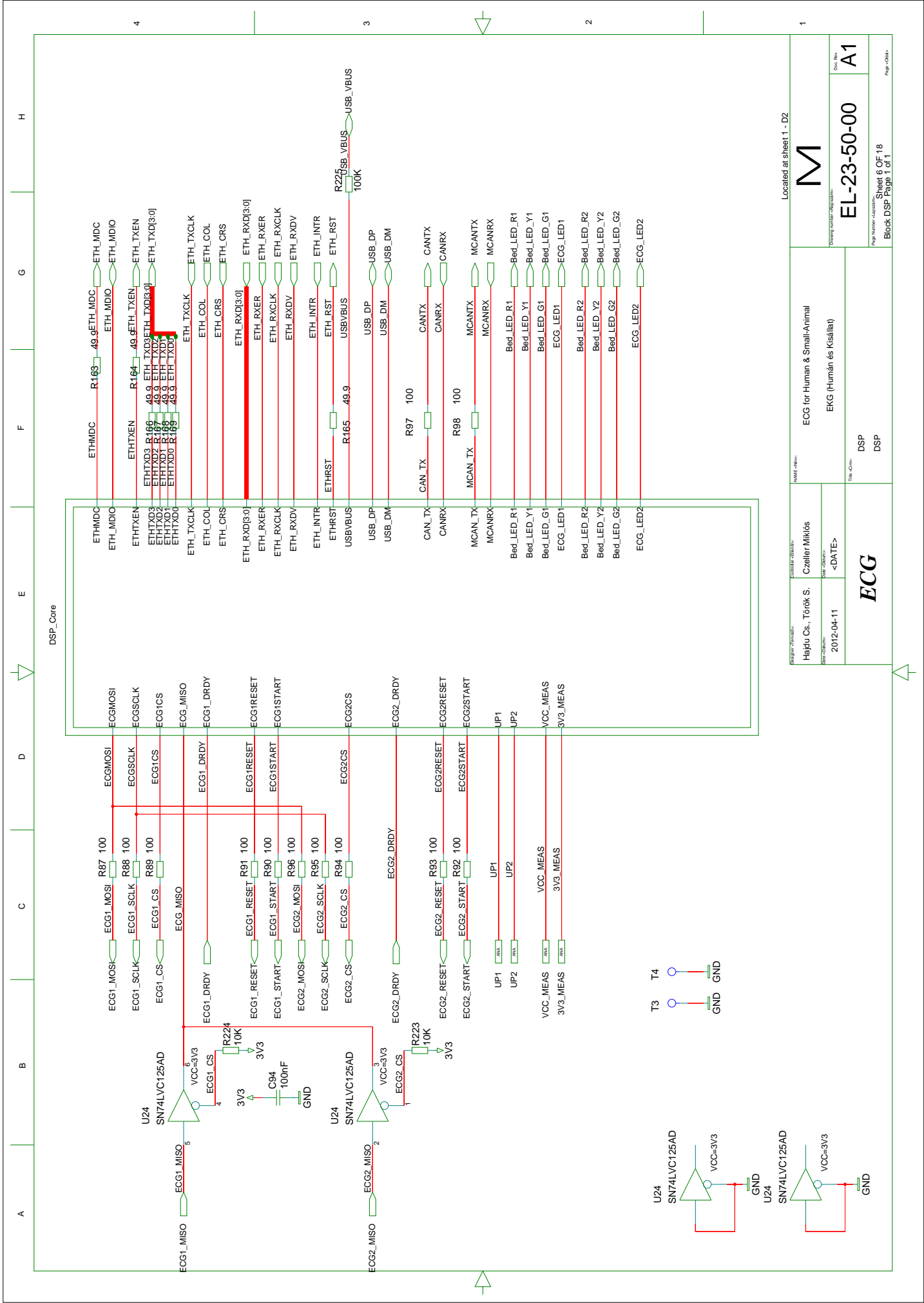
ECG for Human & Small-Animal

EKG (Human és Kisállat)

Power Supplies
Tápegységek



Program: ECG	Project: ECG
Designer: Hejdu Cs., Török S., Czeller Miklós	Customer: ECG for Human & Small-Animal
Date: 2012-04-11	Rev: <DATE>

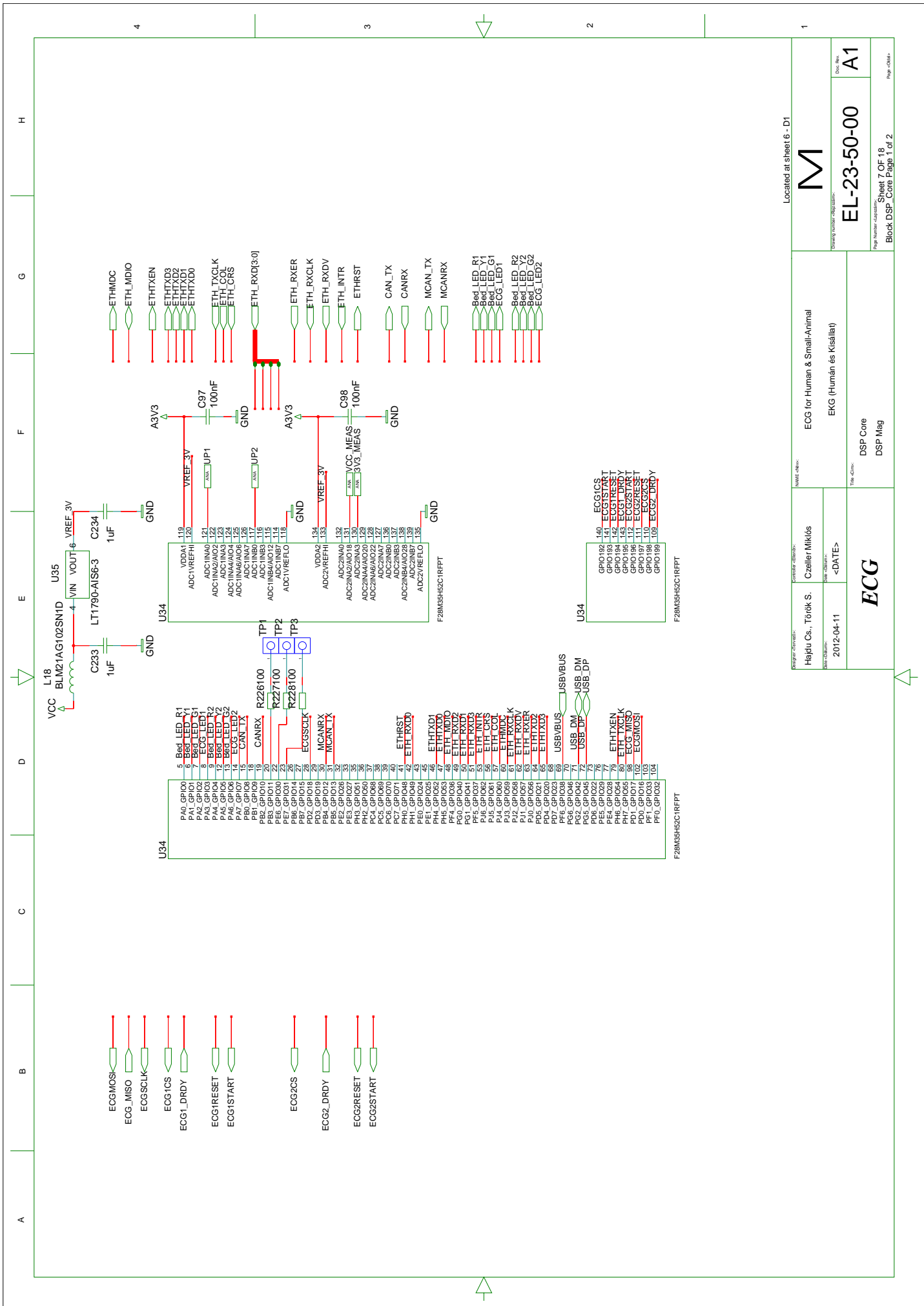


Program: HEMOS Designer: HEMOS Date: 2012-04-11		Project: HEMOS Designer: Czeller Miklós Date: <DATE>		Name: HEMOS Project: ECG for Human & Small-Animal Part: EKG (Humán és Kisállat)		Doc No: A1 Rev: A1	
ECG				DSP DSP		Page Number: 1 of 18 Sheet: 6 of 18 Block DSP: Page 1 of 1	

Located at sheet 1 - D2



EL-23-50-00



Located at Sheet 6 - D1



EL-23-50-00

A1

ECG for Human & Small-Animal

EKG (Humán és Kisállat)

ECG

DSP Core
DSP Mag

Project Name: Czeleler Miklós

Part Number: <DATE>

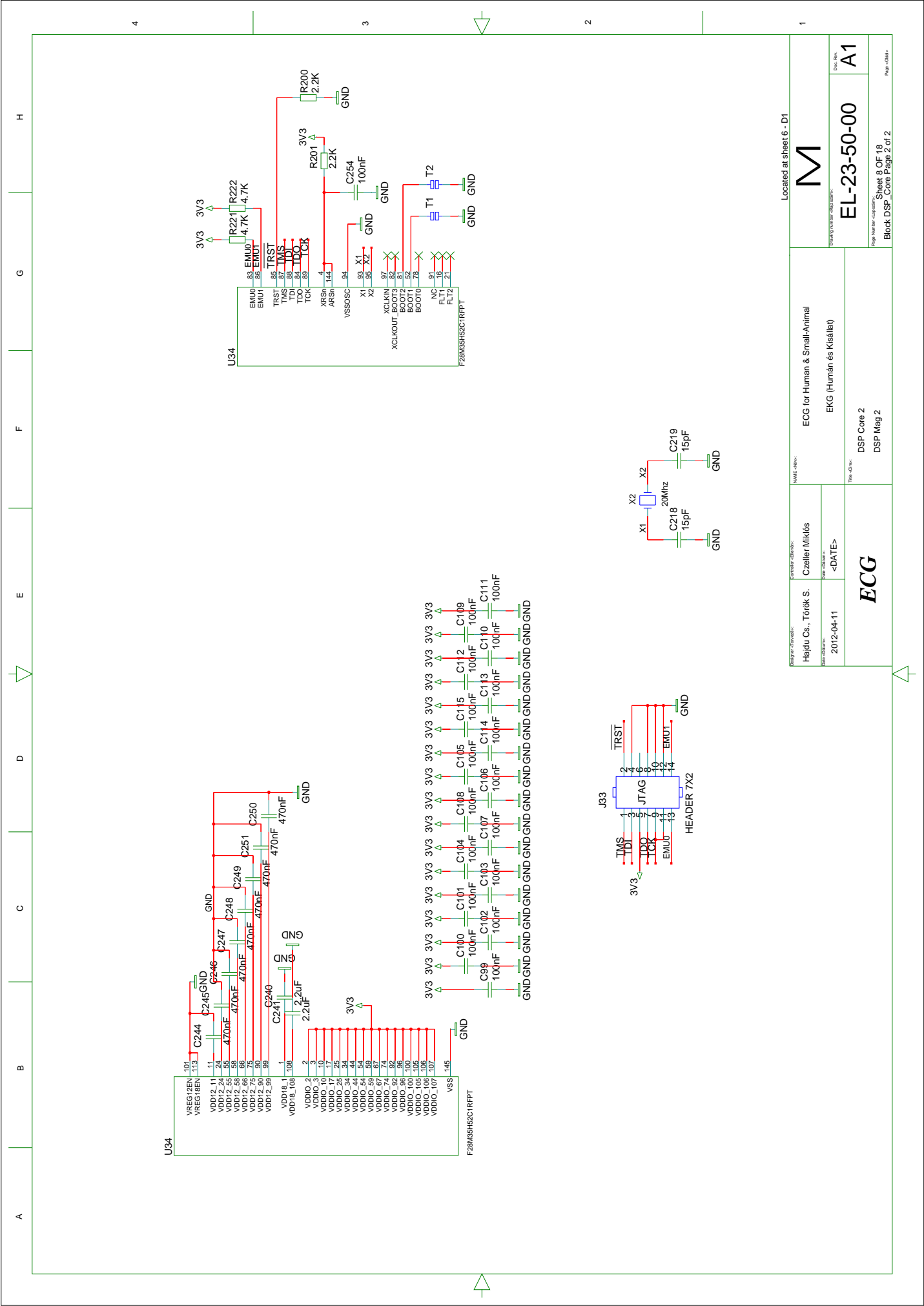
2012-04-11

Revision: 1

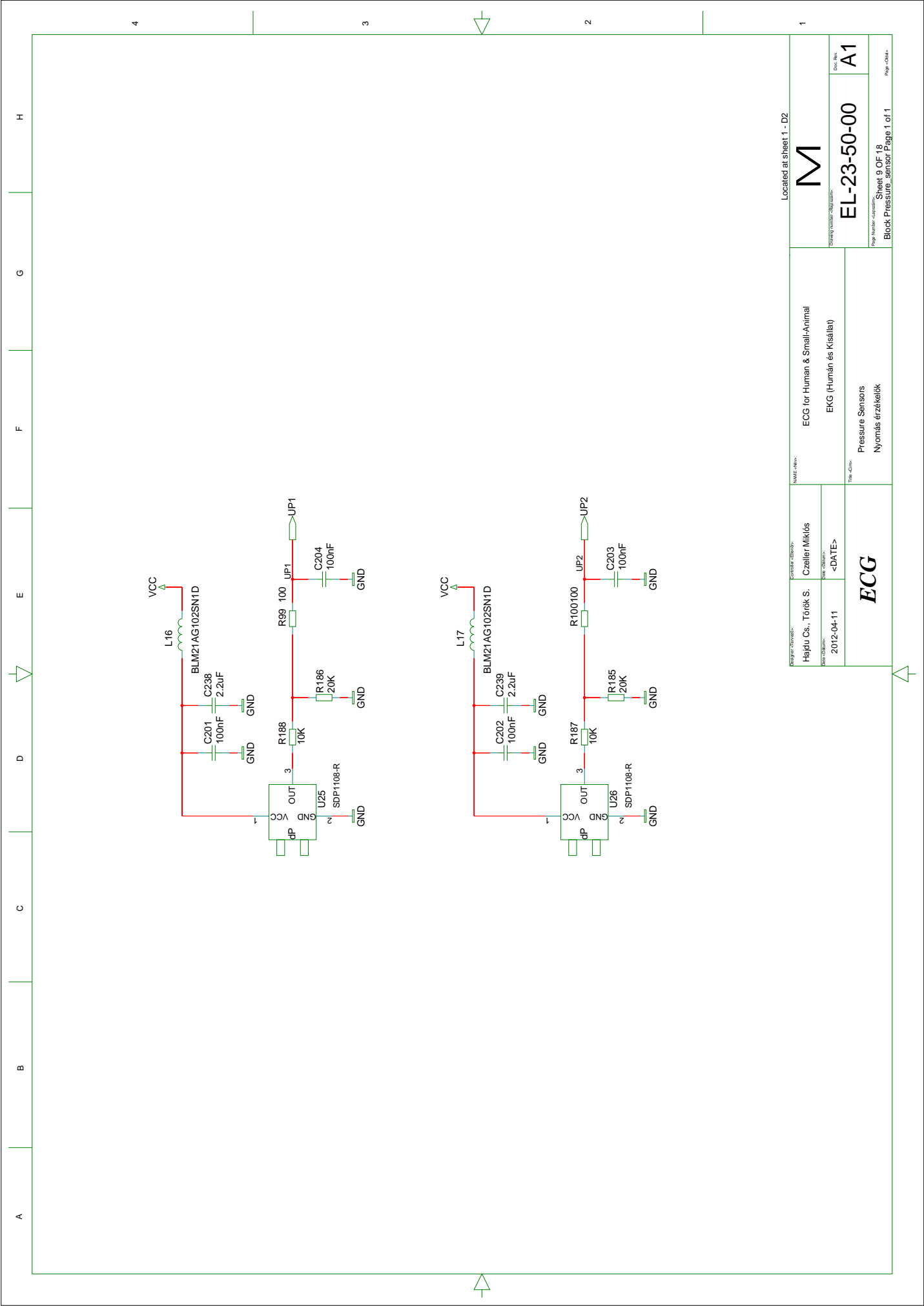
Doc No: A1

Page Number: Sheet 7 OF 18
Block DSP_Core Page 1 of 2

Page 1 of 1



Designer: Hejdu Cs., Török S. Date: 2012-04-11		Customer: Czeller Miklós Part: <DATE>		Name: ECG for Human & Small-Animal Description: EKG (Humán és Kisállat)		Located at Sheet 6 - D1	
Part Number: EL-23-50-00 Revision: A1		Page Number: Sheet 8 OF 18 Block: DSP Core Page 2 of 2		ECG DSP Core 2 DSP Mag 2		Page: 8/18	



Located at sheet 1 - D2

M

ECG for Human & Small-Animal
EKG (Humán és Kisállat)

HEJDU CS., TÖRÖK S., CZELLER MIKLÓS
2012-04-11
-DATE>

ECG

Pressure Sensors
Nyomás érzékelők

EL-23-50-00

A1

Sheet 9 OF 18
Block Pressure_sensor Page 1 of 1

H

G

F

E

D

C

B

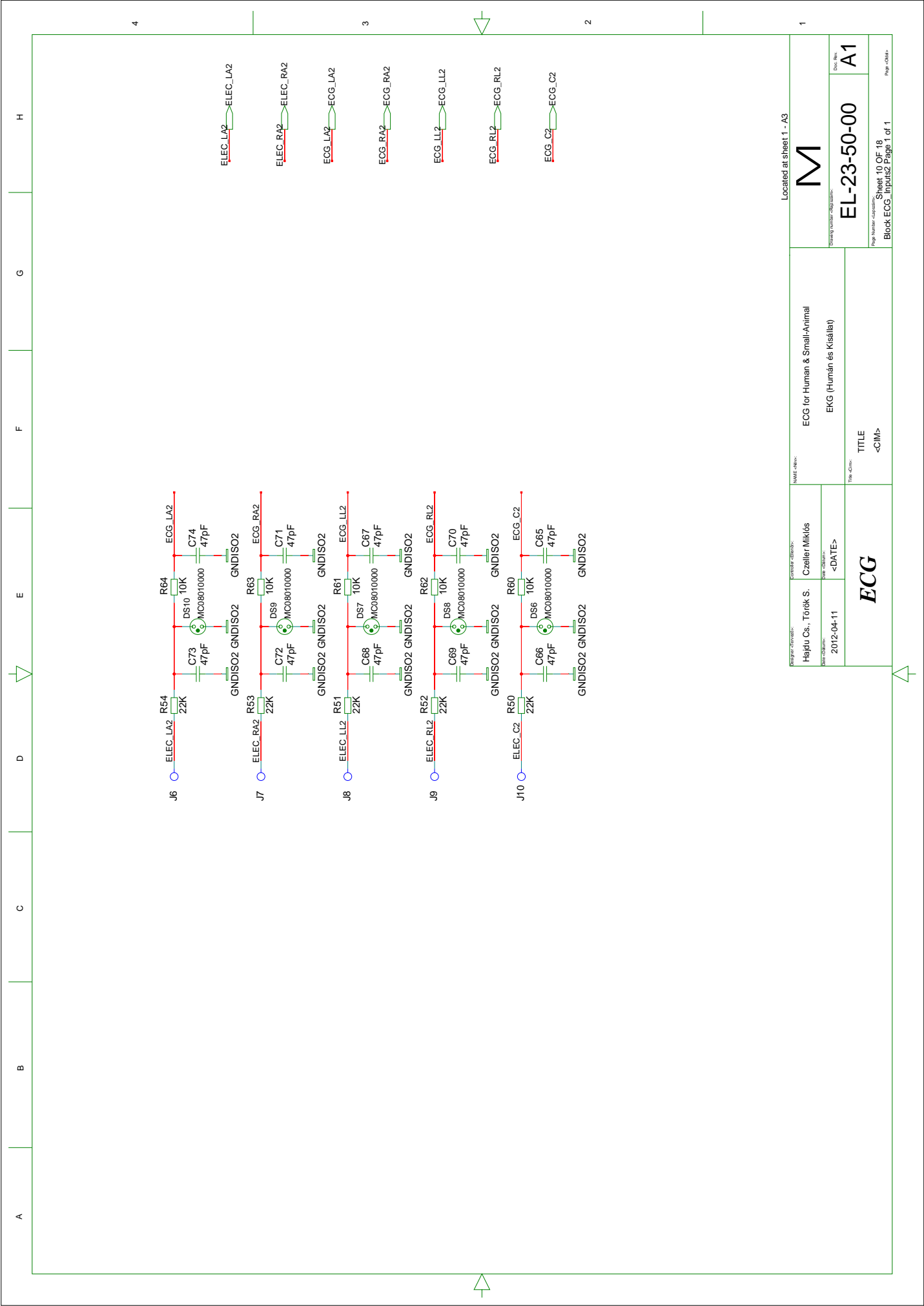
A


4

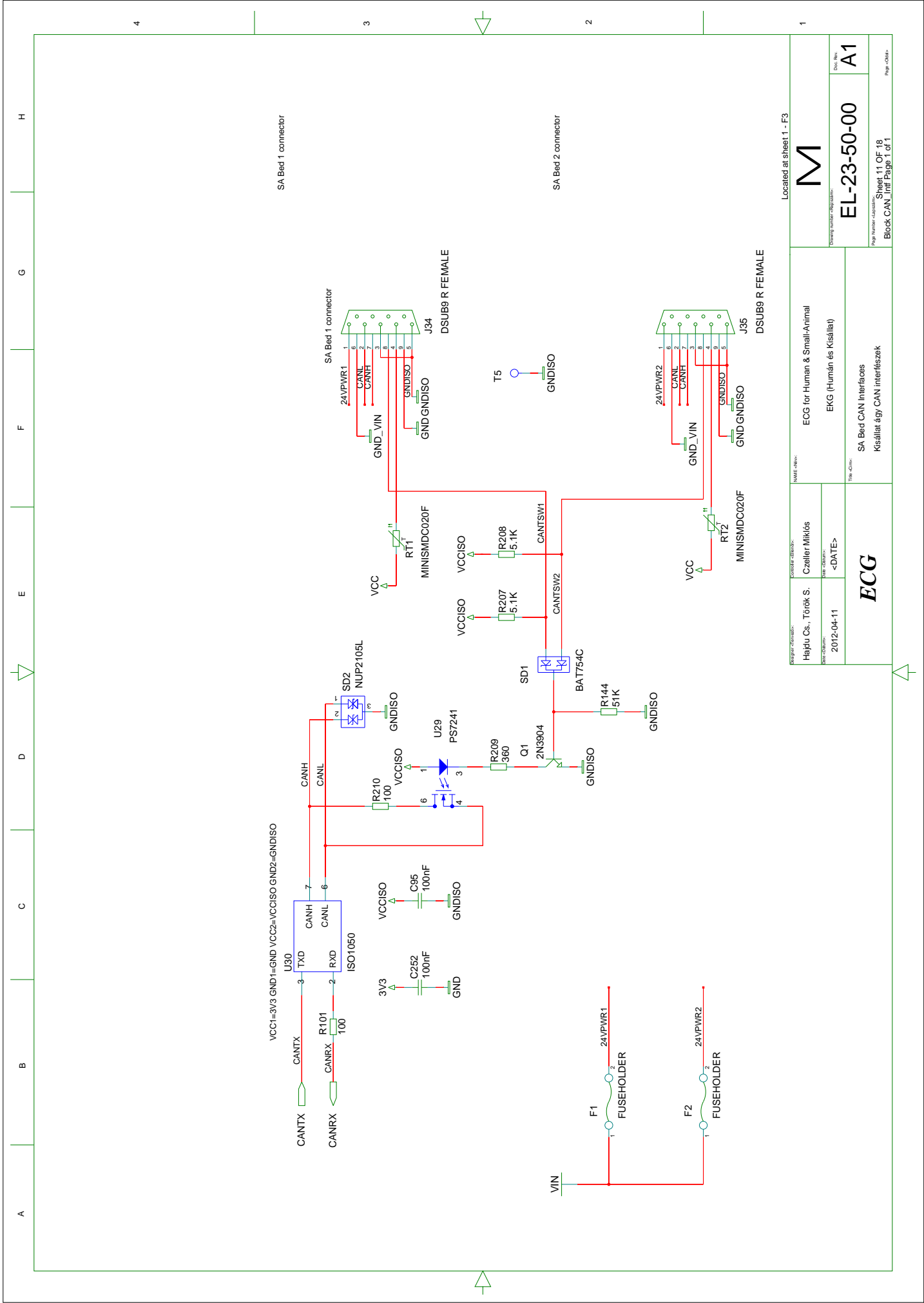
3

2

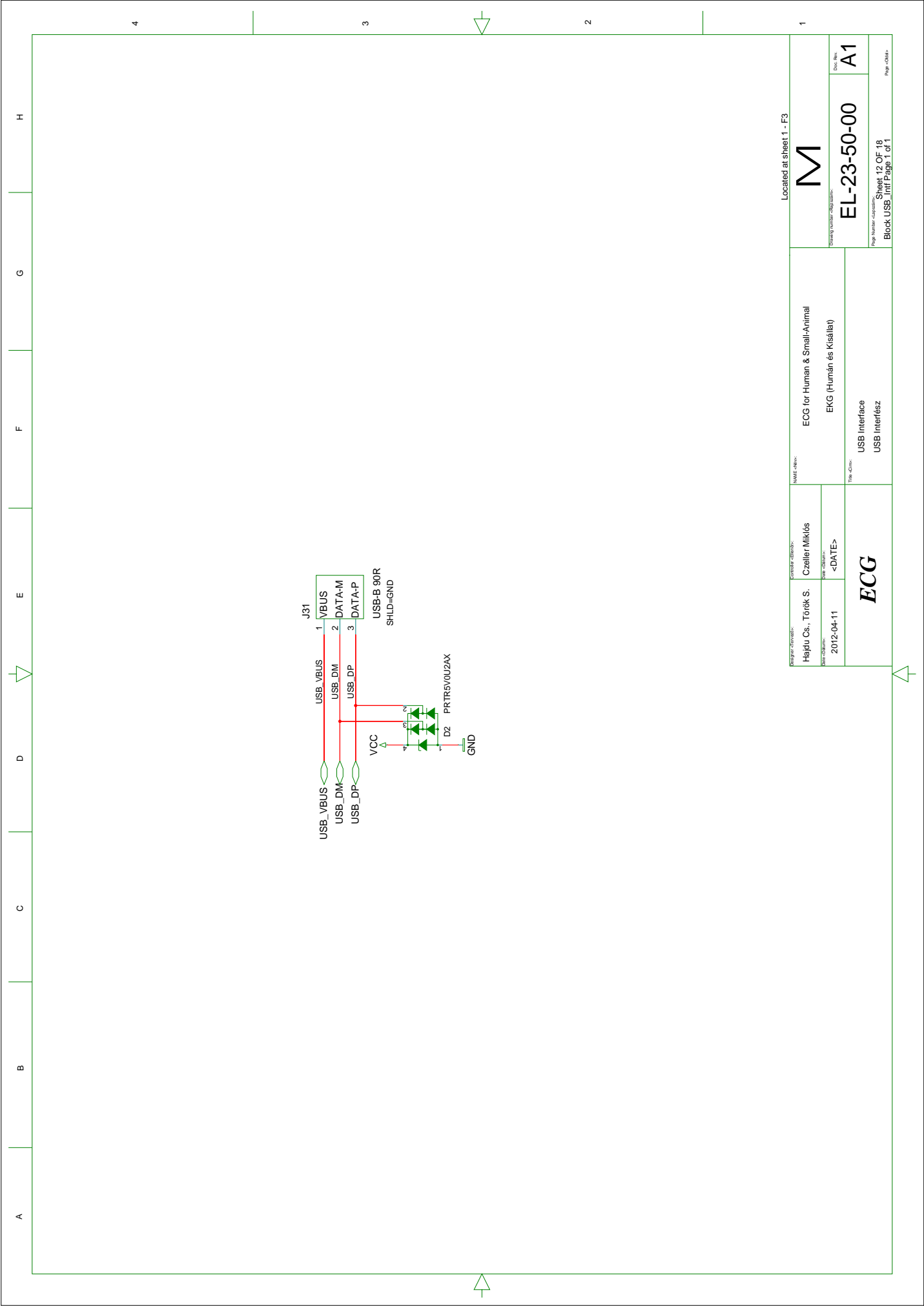
1



Program: HW00000 Designer: HW00000 Date: 2012-04-11		Project: HW00000 Designer: Czeller Miklós Date: <DATE>		Name: HW00000 Description: ECG for Human & Small-Animal Part: EKG (Humán és Kisállat)		Located at Sheet: 1 - A3 	
ECG		Title: <CIM>		Drawing Number: EL-23-50-00 Doc Ref: A1		Page Number: Sheet 10 OF 18 Block ECG Inputs: Page 1 of 1 Page Count: Page 1 of 1	



Program / Revision: ECG Designer: Hejdu Cs., Török S. Date: 2012-04-11 Part: C200001 Rev: <DATE>		Name: ECG for Human & Small-Animal Description: EKG (Humán és Kisállat)		Doc. No.: EL-23-50-00 Rev: A1	
Page: 11 OF 18 Block CAN Intf Page 1 of 1		Title: SA Bed CAN Interfaces Description: Kisállat-ágy CAN interfészek		Located at Sheet 1 - F3	

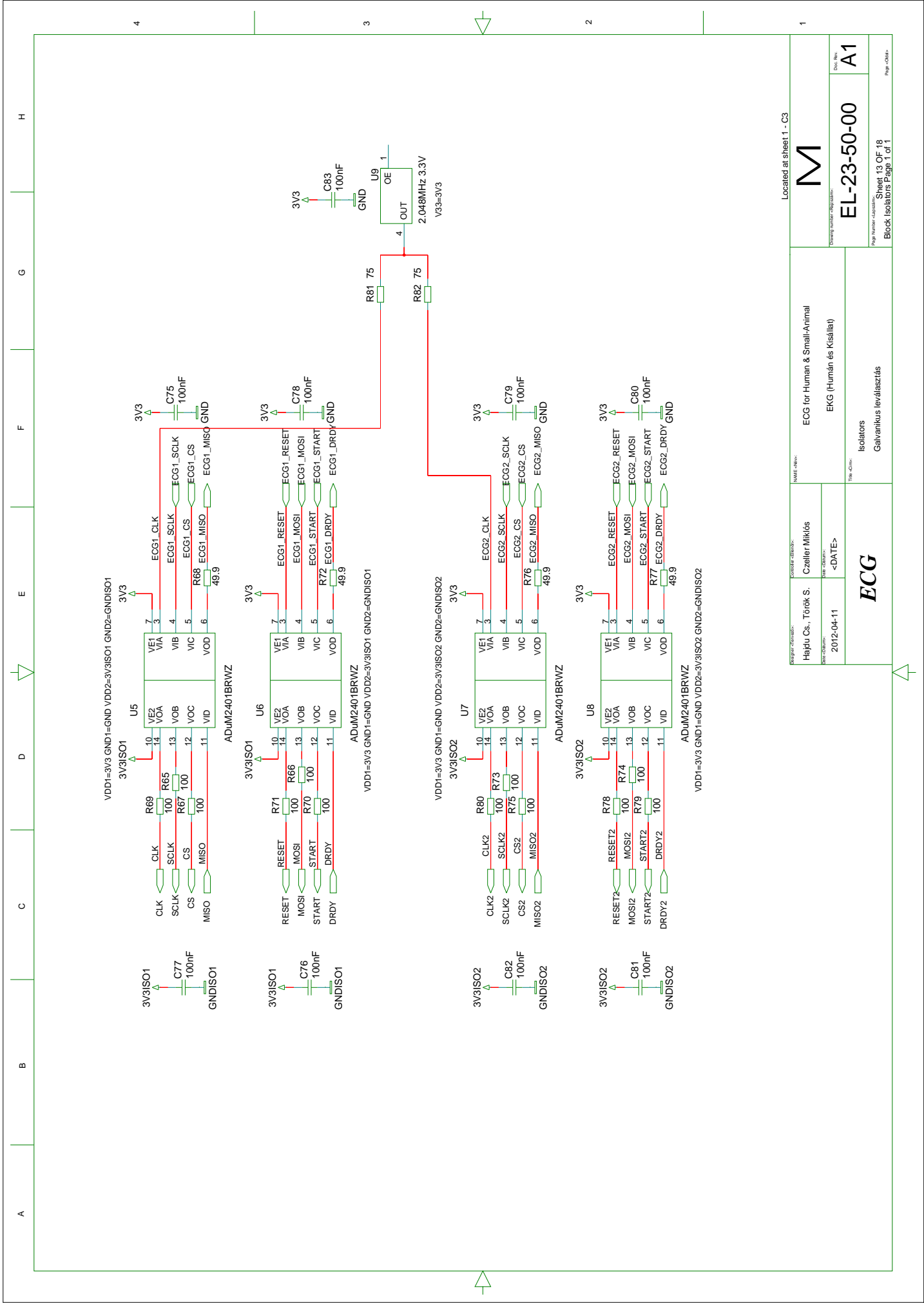


A B C D E F G H

4 3 2 1

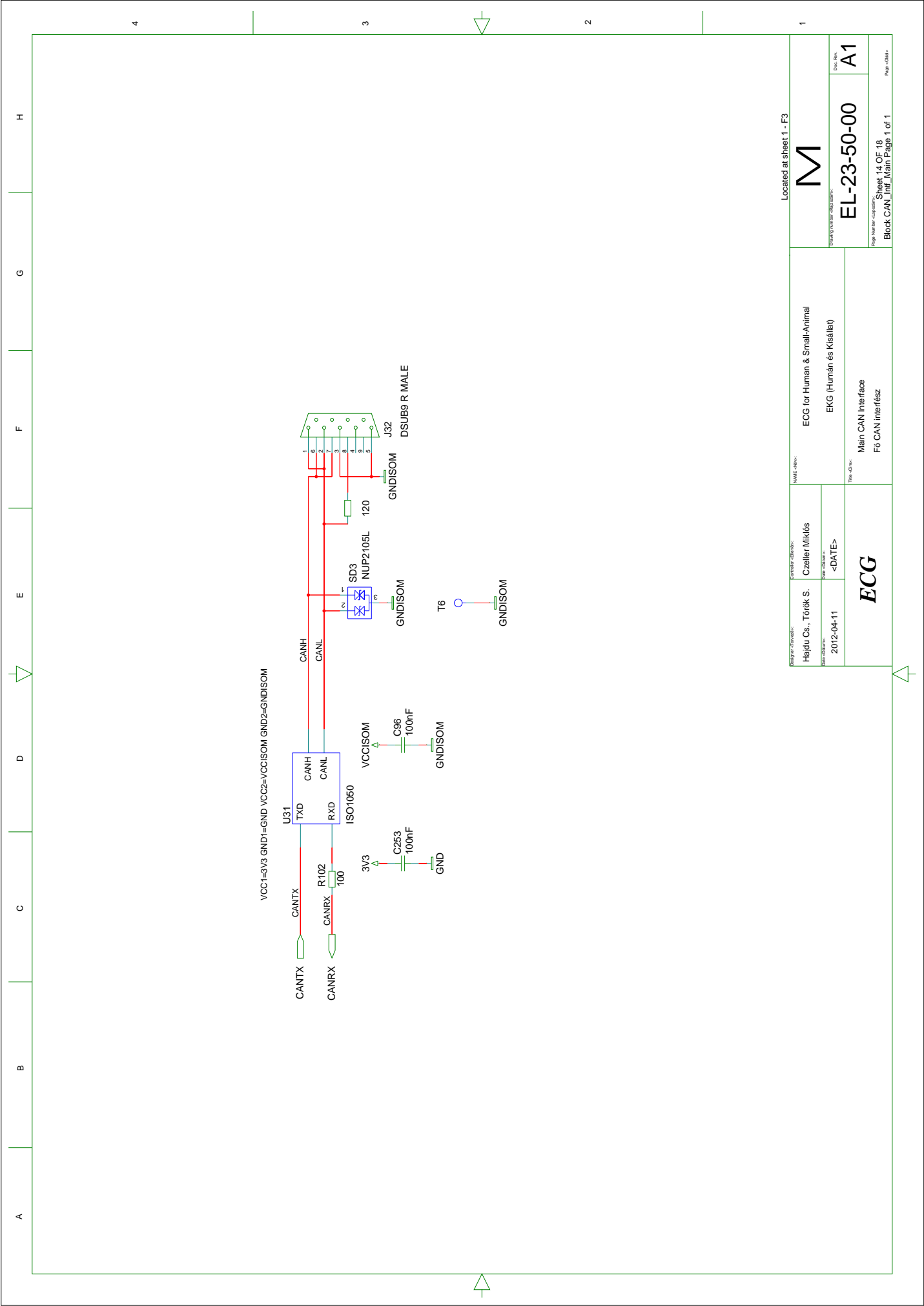
Located at Sheet 1 - F3

ECG		ECG for Human & Small-Animal EKG (Humán és Kisállat)		M EL-23-50-00 Doc. No.	A1 Doc. Rev.
Designer: Hejdu Cs., Török S. Date: 2012-04-11	Designer: Czeller Miklós Date: <DATE>	USB Interface USB Interfész			



Program: ECG Designer: Hejtu Cs., Török S. Date: 2012-04-11		Compiler: Czeller Miklós Name: <DATE>		Name: ECG for Human & Small-Animal EKG (Humán és Kisállat)		Doc No: A1	
ECG				Isolators Galvanikus leválasztás			
Page Number: 18 Sheet: 13 OF 18				Page Number: 18 Sheet: 13 OF 18			
Page: 1				Page: 1			

Located at Sheet 1 - C3

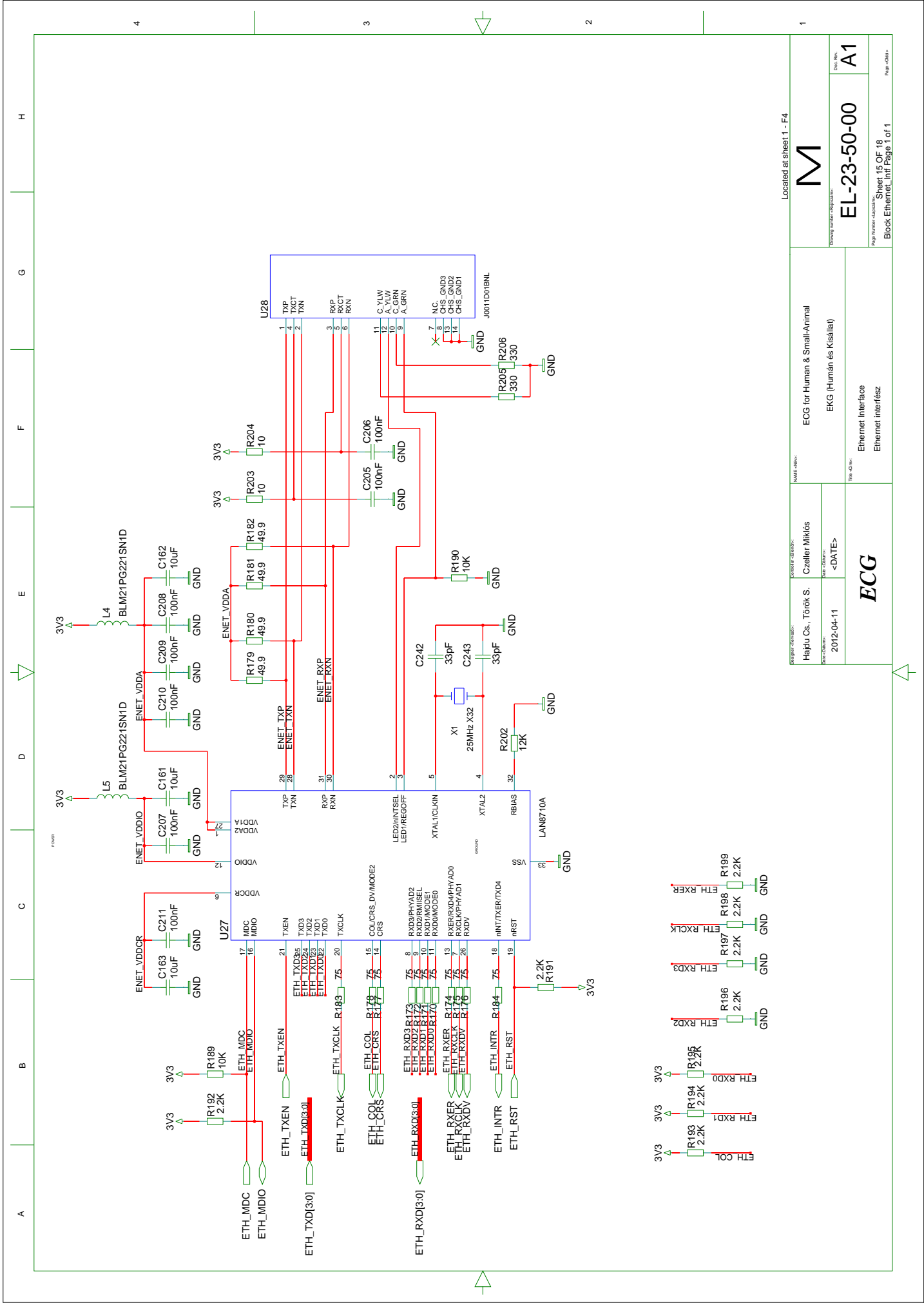


Located at Sheet 1 - F3

M	Doc No:	EL-23-50-00	A1
	Page Number / Sheet / Block CAN Intf. Main Page 1 of 1		

NAME:	ECG for Human & Small-Animal
DESCRIPTION:	EKG (Humán és Kisállat)
TYPE:	Main CAN Interface Fő CAN interfész

DESIGNER:	Czeller Miklós
DATE:	2012-04-11
REVISION:	<DATE>
ECG	



Program: HW00000 Designer: Török S. Date: 2012-04-11		Project: ECG Designer: Czeller Miklós Date: <DATE>		Name: ECG for Human & Small-Animal Description: EKG (Humán és Kisállat)		Located at Sheet 1 - F4 M EL-23-50-00 Sheet 15 OF 18 Block Ethernet_Inf Page 1 of 1	
Part Number: 2012-04-11		Part Name: <DATE>		Part Description: Ethernet Interface Ethernet interfész		Doc No: A1 Page: 15 OF 18	



ECG

Located at Sheet 1 - F4

ECG for Human & Small-Animal

EKG (Humán és Kisállat)

EL-23-50-00

Sheet 15 OF 18

Block Ethernet_Inf Page 1 of 1

Ethernet Interface
Ethernet interfész

ECG

Ethernet Interface
Ethernet interfész

EL-23-50-00

Sheet 15 OF 18

Block Ethernet_Inf Page 1 of 1

ECG for Human & Small-Animal

EKG (Humán és Kisállat)

EL-23-50-00

Sheet 15 OF 18

Block Ethernet_Inf Page 1 of 1

Ethernet Interface
Ethernet interfész

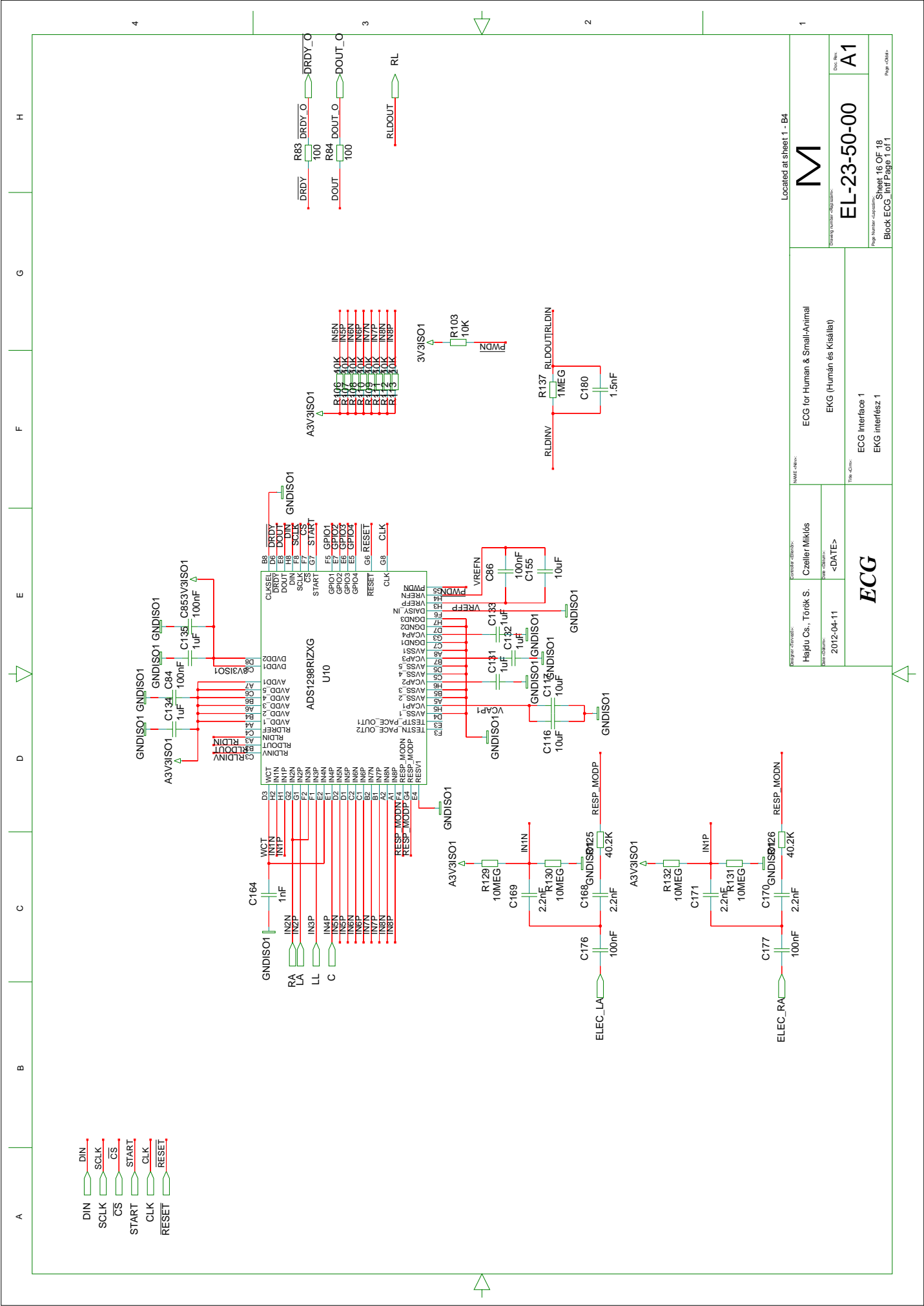
ECG

Ethernet Interface
Ethernet interfész

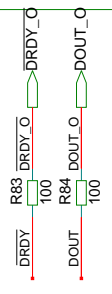
EL-23-50-00

Sheet 15 OF 18

Block Ethernet_Inf Page 1 of 1

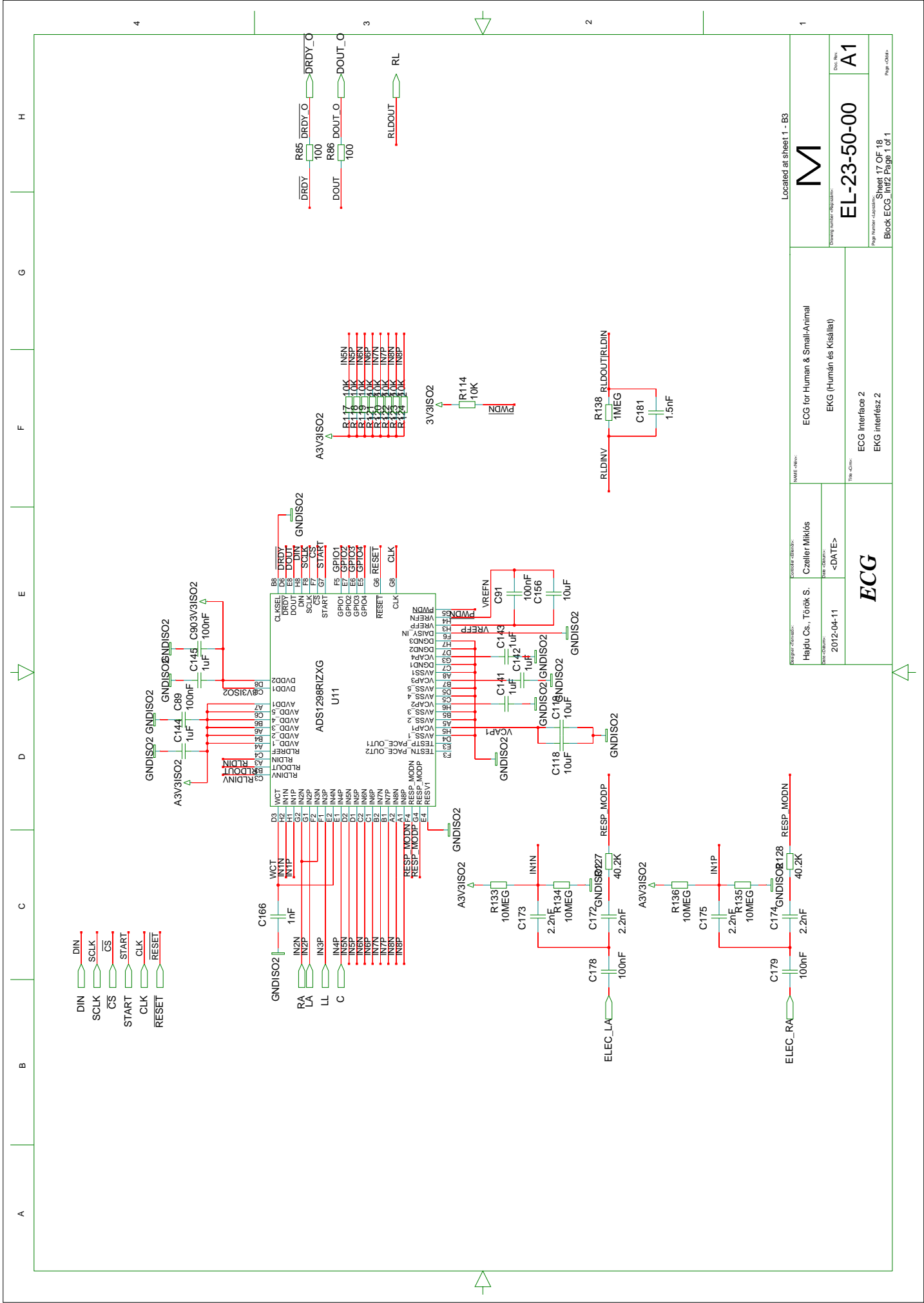


- DIN
- SCLK
- CS
- START
- CLK
- RESET



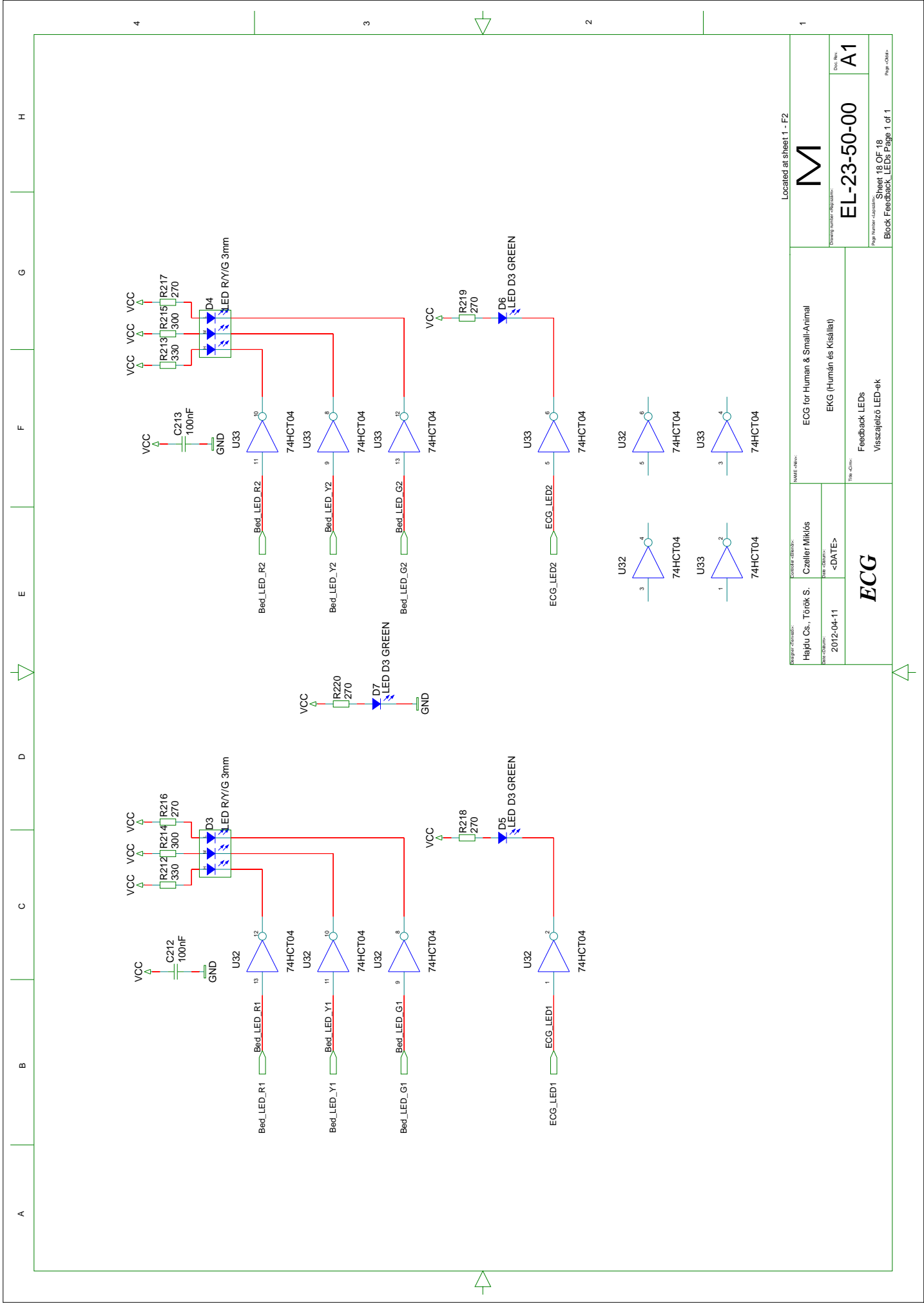
Program: EL-23-50-00 Date: 2012-04-11 Author: Czeleler Miklós		Located at Sheet 1 - B4 ECG for Human & Small-Animal EKG (Humán és Kisállat)	
Part: ECG Interface 1 Title: ECG interfész 1		Doc No: A1 Page Number: 16 OF 18 Block ECG Intf Page 1 of 1	

ECG



Designer: Hejtu Cs., Török S. Date: 2012-04-11		Project: ECG Title: ECG Interface 2 Description: EKG interfész 2	
Designer: Czeller Miklós Date: <DATE>		Project: ECG for Human & Small-Animal Title: EKG (Humán és Kisállat)	
Part Number: EL-23-50-00 Revision: A1		Page Number: Sheet 17 OF 18 Page Count: Block ECG Intf2 Page 1 of 1	

Located at sheet 1 - B3



Located at Sheet 1 - F2



EL-23-50-00

A1

ECG for Human & Small-Animal

EKG (Humán és Kisállat)

ECG

Hejdu Cs., Török S., Czeller Miklós

2012-04-11

<DATE>

Feedback LEDs
Viszajjelző LED-ek

Sheet 18 OF 18
Block Feedback LEDs Page 1 of 1

Page 18 of 18

Page 1 of 1

BIBLIOGRAPHY

- [1] R.E. Klabunde. *Cardiovascular Physiology Concepts*. Wolters Kluwer Health, 2011. ISBN 9781451113846. (Cited on page 1.)
- [2] B. Desjardins and E.A. Kazerooni. ECG-Gated Cardiac CT. *American Journal of Roentgenology*, 182(4):993–1010, 2004. (Cited on page 4.)
- [3] A. Martinez-Moeller et al. Dual cardiac-respiratory gated PET: implementation and results from a feasibility study. *European Journal of Nuclear Medicine and Molecular Imaging*, 34:1447–1454, 2007. ISSN 1619-7070. (Cited on page 4.)
- [4] S. Skare and J.L.R. Andersson. On the effects of gating in diffusion imaging of the brain using single shot EPI. *Magnetic Resonance Imaging*, 19(8):1125 – 1128, 2001. ISSN 0730-725X. (Cited on page 4.)
- [5] Monitoring Patients in the MRI Environment. http://www.mrisafety.com/safety_article.asp?subject=40, . (Cited on page 4.)
- [6] MRI ECG Recording. <http://www.biopac.com/researchApplications.asp?Aid=46&AF=415&Level=3>, . (Cited on page 4.)
- [7] MRI monitor. http://www.gehealthcare.com/euen/patient_monitoring/products/imm-monitoring/datex-ohmeda/mri-monitor/index.html, . (Cited on page 4.)
- [8] Advanced Clinical Solutions For MRI - Precess. <http://www.invivocorp.com/monitors/monitorinfo.php?id=1>, . (Cited on page 4.)
- [9] MRI Small Animal Monitoring. <http://www.biopac.com/researchApplications.asp?Aid=46&AF=417&Level=3>, . (Cited on page 4.)
- [10] Model 1030 Monitoring & Gating System. http://www.i4sa.com/web_app/main/defaultProduct.aspx?ID=76&PT=3, . (Cited on pages 4 and 33.)
- [11] ECG Front-End Design is Simplified with MicroConverter. <http://www.analog.com/library/analogDialogue/archives/37-11/ecg.pdf>. (Cited on page 8.)

- [12] Heart-Rate and EKG Monitor Using the MSP430FG439. <http://www.ti.com/lit/an/slaa280a/slaa280a.pdf>. (Cited on page 8.)
- [13] ECG Implementation on the TMS320VC5505 DSP Medical Development Kit (MDK). <http://www.ti.com/lit/an/sprab36b/sprab36b.pdf>, . (Cited on pages 8, 12, and 13.)
- [14] Competing ECG AFEs Reveal Chipmakers' New Business Paradigms. <http://electronicdesign.com/article/analog-and-mixed-signal/competing-ecg-afes-reveal-chipmakers-new-business-paradigms>. (Cited on page 8.)
- [15] Low-Power, 8-Channel, 24-Bit Analog Front-End for Biopotential Measurements - datasheet. <http://www.ti.com/lit/ds/symlink/ads1298r.pdf>, . (Cited on pages 8, 9, 15, 24, and 25.)
- [16] J Pan and W J Tompkins. A real-time QRS detection algorithm. *IEEE Transactions on Biomedical Engineering*, 32(3):230–236, March 1985. (Cited on page 19.)
- [17] Concerto™ Dual-Subsystem MCU Series | 28x + ARM® Cortex™-M3. <http://www.ti.com/mcu/docs/mcuproductcontentnp.tsp?sectionId=95&familyId=2049&tabId=2743>, . (Cited on page 21.)
- [18] TEN 5WI Series, 6 Watt DC/DC converters - datasheet. <http://www.tracopower.com/products/ten5wi.pdf>, . (Cited on page 23.)
- [19] DC/DC-Converter 2 Watt DIP24 Miniature Single & Dual Output - datasheet. <http://www.recom-international.com/pdf/Econoline/RV.pdf>. (Cited on page 23.)
- [20] Ultralow-noise, high PSRR, fast RF 100-mA low-dropout linear regulators - datasheet. <http://www.ti.com/lit/ds/slvs337b/slvs337b.pdf>, . (Cited on page 23.)
- [21] TME Series, 1 Watt DC/DC converters - datasheet. <http://www.tracopower.com/products/tme.pdf>, . (Cited on page 23.)
- [22] Ultralow-noise, high PSRR, fast, RF, 1A low-dropout linear regulators - datasheet. <http://www.ti.com/lit/ds/slvs351n/slvs351n.pdf>, . (Cited on page 23.)
- [23] Quad-Channel Digital Isolators. http://www.analog.com/static/imported-files/data_sheets/ADuM2400_2401_2402.pdf. (Cited on page 24.)
- [24] ADS1298R ECG Front-End Performance Demonstration Kit User's Guide. <http://www.ti.com/lit/ug/sbau181/sbau181.pdf>, . (Cited on page 24.)

- [25] multcomp Wire Ended T1 1/4 Neon lamps - datasheet. <http://www.farnell.com/datasheets/320136.pdf>. (Cited on page 24.)
- [26] SDP1108/SDP2108 Low Differential Pressure Sensor with fast response time - datasheet. http://www.sensirion.com/en/pdf/product_information/Datasheet_differential_pressure_sensor_SDP1108_SDP2108.pdf. (Cited on page 25.)
- [27] Concerto Microcontrollers - datasheet. <http://www.ti.com/lit/ds/symlink/f28m35h52c.pdf>. (Cited on page 26.)
- [28] Concerto Control Card - F28M35xx - schematics. Available through TI's ControlSuite, <http://www.ti.com/tool/controlsuite>, . (Cited on page 26.)
- [29] Isolated CAN Transceiver - datasheet. <http://www.ti.com/lit/ds/symlink/iso1050.pdf>. (Cited on page 26.)
- [30] Biology of the Rat. <http://www.lvma.org/rat.html>, . (Cited on page 31.)
- [31] Biology of the Hamster. <http://www.lvma.org/hamster.html>, . (Cited on page 33.)
- [32] Westbrook, C. and Roth, C.K. and Talbot, J. *MRI in Practice*. John Wiley & Sons, 2011. ISBN 9781118273869. (Cited on page 33.)